Vib–rotational energy distributions and relaxation processes in pulsed HF chemical lasers

A. Ben-Shaul*

Department of Chemical Physics, The Weizmann Institute of Science, Rehovot, Israel

K. L. Kompa and U. Schmailzl

Max-Planck Institute für Plasmaphysik, Euratom Association, 8046 Garching bei München, Federal Republic of Germany

(Received 20 October 1975)

The rate equations governing the temporal evolution of photon densities and level populations in pulsed $F+H_2 \rightarrow HF+H$ chemical lasers are solved for different initial conditions. The rate equations are solved simultaneously for all relevant vibrational–rotational levels and vibrational–rotational P-branch transitions. Rotational equilibrium is not assumed. Approximate expressions for the detailed state-to-state rate constants corresponding to the various energy transfer processes (V–V, V–R,T, R–R,T) coupling the vib–rotational levels are formulated on the basis of experimental data, approximate theories, and qualitative considerations. The main findings are as follows: At low pressures, R–T transfer cannot compete with the stimulated emission, and the laser output largely reflects the nonequilibrium energy distribution in the pumping reaction. The various transitions reach threshold and decay almost independently and simultaneous lasing on several lines takes place. When a buffer gas is added in excess to the reacting mixture, the enhanced rotational relaxation leads to nearly single-line operation and to the J shift in lasing. Laser efficiency is higher at high inert gas pressures owing to a better extraction of the internal energy from partially inverted populations. V–V exchange enhances lasing from upper vibrational levels but reduces the total pulse intensity. V–R,T processes reduce the efficiency but do not substantially modify the spectral output distribution. The photon yield ranges between 0.4 and 1.4 photons/HF molecule depending on the initial conditions. Comparison with experimental data, when available, is fair.

I. INTRODUCTION

The hydrogen fluoride chemical laser based on the reaction

$$F+H_2 \rightarrow HF(V,J)+H \qquad \text{(R. 1)}$$

has received a great deal of attention since its discovery in 1966.[1,2] This is motivated, in part, by the fact that it is one of the more promising systems for high energy operation. Indeed, both in continuous wave and pulsed HF lasers, output levels in the multikilowatt and multikilojoule ranges have been demonstrated.[3] Considerable problems arise, however, from their extremely high radiational and collisional losses, which result in a very complex and rapidly changing gain distribution over the vib–rotational manifolds.

The general aim of this paper is to investigate individual and mutual effects of various kinetic processes (pumping, stimulated radiation, and relaxation) on the operation of pulsed chemical lasers in general and the HF laser in particular. To this end we have solved, for various initial conditions, the rate equations governing the temporal evolution of level populations and photon densities in the laser cavity. In order to study the effects of rotational disequilibrium and vibration to rotation energy transfer processes, we have not assumed *a priori* rotational equilibrium. (We compare two rather extreme pressure ranges: Low, where rotational relaxation is moderate, and high—due to a buffer gas—where rotational relaxation is fast.)

The rate equations include all the relevant vib–rotational levels and radiative transitions. The main limitation of this approach is in the lack of detailed information about all the relevant state-to-state rate constants. Another problem is the lack of precision of (low pressure) laser output measurements against which the theoretical results can be compared.

The assumption of instantaneous rotational relaxation enables one to consider only one (the "highest gain") radiative transition between each pair of vibrational levels at a time. In addition, it implies that only vibrational populations and vibrational energy transfer processes must be included in the rate equations. Model calculations[4–11] based on these approximations have been performed for various chemical laser systems and have made a major contribution to the understanding of their dynamic behavior. Yet the common observation of simultaneous lasing on several vib–rotational lines is just one indication that, at least under certain conditions (e.g., low pressures), rotational equilibrium is not maintained throughout the laser pulse.

The role of rotational nonequilibrium in chemical lasers has been investigated in several recent model calculations.[14–19] Padrick and Gusinow[15] included the R–T processes in a model of the $HF(CF_3I+N_2F_4)$ chemical laser and found that the assumption of a Boltzmann rotational distribution is a poor approximation to the experimental data.[13] In their work on atmospheric pressure-pulsed HF (H_2–F_2) lasers, Chen *et al.*[16] have considered two different initial rotational distributions (thermal and "frozen"). Taking into account vibrational (but not rotational) relaxation they found, as expected, that the two laser outputs are markedly different. Sentman[17] studied the effects of rotational nonequilibrium on cw HF lasers. Using a detailed, two (vibrational) level model he found, for instance, that lasing can occur simultaneously on several lines. A detailed modelling of

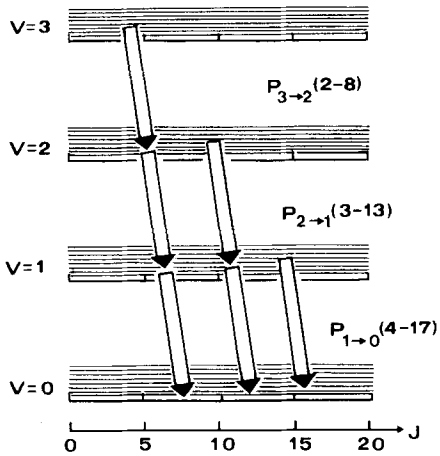

FIG. 1. Schematic illustration of the output pattern observed in low pressure pulsed HF lasers (Ref. 8, 12). $P_{3\to2}$ (2–8), etc., indicate the range of observed transitions. Arrows indicate maxima in the spectrum.

the pulsed Cl + HBr → HCl + Br in which the effects of rotational disequilibrium are systematically analyzed has recently been performed by Keren *et al.*[18] It was found, among others, that rotational relaxation enhances the lasing intensity and that single line operation occurs only at high pressures.

In a preceding paper[14] we carried out a simple model calculation for a low pressure pulsed HF laser. Pumping and radiation into, and from, all the vib–rotational levels were taken into account, but relaxation processes were ignored. This was an attempt to explain some experiments[12] in which transitions from highly excited rotational levels have been observed,[20] Fig. 1. Moreover, certain transitions originate from rotational levels which, according to the chemiluminescence measurements of Polanyi and Woodall[21] are not populated by (R. 1). Some features of the laser output were correctly reproduced when a simple statistical model[22] (which, like some trajectory computations,[23] predicts the population of high rotational levels) was used to describe the nascent rotational product distribution in (R. 1). However, the possibility that the lasing from the highest rotational levels was, partly or completely, due to secondary relaxation and pumping processes could not be ruled out. The opposite ways in which V–R, T and R–R, T processes affect the laser output may serve as an example illustrating this point. The V–R processes can generate HF molecules in highly excited rotational levels. This will be reflected in the laser output only if the rates of V–R transfer into, and stimulated emission out of, these levels can effectively compete with their depletion by R–T relaxation. In view of the indications[26,27] that the rate of R–T transfer decreases rapidly with J this possibility seems quite probable.

II. MODEL

A. Rate equations

As in previous studies,[4–9,14–19] the interaction of the radiation field with the molecules is treated here in the rate equation approximation.[28] The pumping, relaxation, and radiation are taken to be uniform along the laser axis so that the level populations and photon densities are functions of time only. Except under very unusual conditions of rotational nonequilibrium, the gain corresponding to the P-branch transition, $V,J \to V-1$, $J+1$ is higher than the gain in the R-branch transition originating from the same level $(V,J \to V-1,J-1)$. In a "free running" laser experiment very few R-branch transitions can, transiently, lase.[18] Thus, only P-branch transitions will be considered.

Using N_{VJ} to denote the density of HF(V,J) molecules and q_{VJ} for the density of photons in the transition $V,J \to V-1,J+1$, the rate equations are of the form

$$\frac{dN_{VJ}}{dt} = P_{VJ} - A_{VJ}N_{VJ} + A_{V+1,J-1}N_{V+1,J-1} - c\sigma_{VJ}\Delta N_{VJ}q_{VJ} + c\sigma_{V+1,J-1}\Delta N_{V+1,J-1}q_{V+1,J-1} - L_{VJ}\ , \tag{1}$$

$$\frac{dq_{VJ}}{dt} = \alpha A_{VJ}N_{VJ} + c\sigma_{VJ}\Delta N_{VJ}q_{V,J} - \frac{q_{VJ}}{\tau}\ , \tag{2}$$

where $\Delta N_{VJ} = N_{VJ} - [(2J-1)/(2J+3)]N_{V-1,J+1}$ is the population inversion; P_{VJ} is the rate of pumping into VJ; A_{VJ} is the Einstein coefficient for spontaneous emission; σ_{VJ} is the cross section for stimulated emission out of VJ; L_{VJ} symbolizes the net loss of HF(VJ) molecules due to all nonradiative processes; τ is the photon lifetime in the cavity; c is the speed of light; and α is the (average) fraction of spontaneously emitted photons which ignite the lasing.

In all, 144 equations are included in the calculations, 84 for vib–rotational levels ($V=0-3, J=0-20$ in each V) and 60 for the P-branch photon densities.

1. Radiation

The spontaneous emission terms are important only before threshold. Their influence on N_{VJ} via (1) is negligible. In (2) they provide a noise level of photons to start the amplification process. The constant α is the effective fraction of photons emitted into the solid angle confined by the laser cavity (the fraction of photons corresponding to stable cavity modes). Practically, owing to the very fast growth in photon density near threshold the results of the calculations are not sensitive to α. We have taken $\alpha = 10^{-4}$.

For the range of pressures considered in this work (usually $P \sim 1$ torr), the spectral lines are mainly Doppler broadened, and the cross section of a vib–rotational transition, at line center, is given by

$$\sigma_{VJ} = \sigma_{VJ\to V-1,J+1} = (4\ln 2/\pi)^{1/2}(c^2/8\pi\nu_{VJ}^2)^{-1}\Delta\nu_D^{-1}A_{VJ\to V-1,J+1}\ , \tag{3}$$

with $\Delta\nu_D = (8kT\ln 2/m)^{1/2}\nu_{VJ}/c$. The numerical values o σ were calculated on the basis of known A coefficients.[25] For $T = 300\,^{\circ}$K, the value employed in calculating σ_{VJ} (see below), $\Delta\nu_D \simeq 10^{-2}$ cm^{-1} and $\sigma_{VJ} \sim 10^{-15}$ cm^2. Although the lines are mainly Doppler broadened, the power extraction is taken to be homogeneous over the entire line profile. This seems to be justified for lasers with low quality factor and overlapping cavity modes. In view of the presently available, rather in-

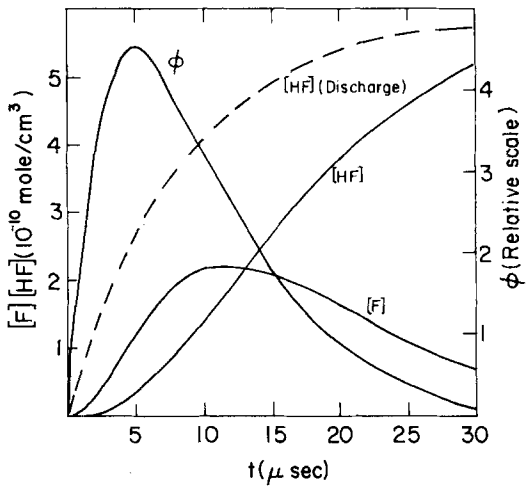

FIG. 2. Time dependence of flash intensity ϕ, F and HF concentration for flash initiation, calculated from Eqs. (8), (9), and (10), respectively. The time dependence of HF concentration for discharge initiation, calculated from Eq. (6) for initial F: H_2 = 1: 10, is shown for comparison.

accurate, experimental data no attempt was made to correct for any finer optical or spectroscopic details of the laser.

We disregarded all cavity losses except for output coupling. The power of the laser is thus determined by q_{vJ}/τ in (2). In all the calculations we have used $\tau = 10^{-7}$ sec. For a 200 cm long optical cavity with one completely reflecting mirror, this value of τ corresponds to a round trip output coupling of ~ 15%. The total output energy radiated in a single vib–rotational transition, per 1 cm^3 of active laser volume, is given by

$$I_{vJ} = h\nu_{vJ} q_{vJ} = \frac{h\nu_{vJ}}{\tau} \int_{\tau_{th}}^{\tau_q} q_{vJ}(t)dt \,, \tag{4}$$

where τ_{th} and τ_q are the thresholds and quenching times, respectively. The threshold inversion can be estimated from $\Delta N_{th} = (c\sigma\tau)^{-1}$, i.e., $\Delta N_{th} \sim 10^{11}$–$10^{12}$ molecule/cm^3, which, at ordinary temperatures, corresponds to a pressure difference of $\Delta P_0 \sim 10^{-5}$ torr.

2. *Initial conditions*

In order that the model calculations will be applicable to experimental situations, the following technical conditions are assumed.

(i) Reagent mixture: Two initial reactant concentration ratios are considered: F: H_2 = 1: 10 and 5: 6. While the initial H_2 concentration is kept constant, $[H_2] = 6\times10^{-9}$ mole/cm^3, the final [HF] in both cases is 6×10^{-10} and 5×10^{-9} mole/cm^3, respectively. (At $T = 300\,^\circ$K, 6×10^{-9} mole/cm^3 corresponds to ~ 0.1 torr.) Some of the calculations will apply to the case where buffer gas is added in excess to the system to enhance rotational thermalization. In both F: H_2 compositions, $[SF_6] = [H_2]$.

(ii) Initiation: Two mechanisms for generating F atoms are considered:

(a) Fast; the fluorine atom production is completed at $t < 1$ μsec. This case resembles the situation in fast electrically pumped lasers[12,30] (e.g., via $SF_6 + e^- \rightarrow SF_5 + F + e^-$), and we shall refer to it as "discharge." The time dependences of N_F, N_{H_2}, N_H, and $N_{HF} \equiv \sum N_{vJ}$ are determined by

$$-dN_F/dt = k_1 N_F N_{H_2} \,, \tag{5}$$

where only the forward process in (R. 1) is considered [see (b) below]. Thus

$$N_{H_2} = N_{H_2}(0) - X = A - X, \quad N_F = N_F(0) - X = B - X \,,$$
$$N_{HF} = X = \frac{A\{\exp[k_1(A-B)t] - 1\}}{\{(A/B)\exp[k_1(A-B)t] - 1\}} \,. \tag{6}$$

The half-life times of the reaction for $A:B = 1:10$ and 5: 6 are 4 and 8 μsec, respectively ($B = 6\times10^{-9}$ mole/cm^3), Fig. 2.

(b) Slow; gradual production of F atoms, for example by flashphotolysis. We refer to this kind of pumping as "flash." In this case

$$dN_F/dt = \phi(t) - k_1 N_F N_{H_2} \,, \quad dN_{HF}/dt = k_1 N_F N_{H_2} \,, \tag{7}$$

where $\phi(t)$ is the rate of photolysis. If, as in Ref. 31, only a small fraction of the fluorine rich molecules (e.g., CF_3I) are photolized, then $\phi(t) \simeq N_{CF_3I}\phi'(t)$, where $\phi'(t)$ is the flash profile. We have taken

$$\phi(t) = at\exp(-bt) \,, \tag{8}$$

with $a = 24$ mole/$cm^3 \cdot$ sec^2 and $b = 2\times10^5$ sec^{-1}. $\phi(t)$ obtains its maximum at $t = 5$ μsec and has a width of ~ 10 μsec, which compares well with the data of Ref. 31. The choice of a and b is consistent with the requirement that $\int\phi(t)dt = 6\times10^{-10}$ mole/cm^3, i.e., that [in the absence of (R. 1)] the total number of F atoms produced by the flash will be identical to $N_F(0)$ in the case of discharge initiation for F: H_2 = 1: 10. (This is, approximately, also the reactant ratio in Ref. 31.) Insertion of (7) into (8) yields

$$N_F(t) = \frac{a}{(b-k)^2}\exp(-bt)[\exp(b-k)t - (b-k)t - 1] \tag{9}$$

$$N_{HF}(t) = \frac{a}{(b-k)^2}[1 - \exp(-kt)] - \frac{ak(2b-k)}{b^2(b-k)^2} \times[1 - \exp(-bt) + \frac{ak}{b(b-k)}t\exp(-bt) \,, \tag{10}$$

where $k = k_1 N_{H_2}(0) = 1.2\times10^5$ sec^{-1}. $\phi(t)$, $N_F(t)$, and $N_{HF}(t)$ are shown in Fig. 2. The F: H_2 = 5: 6 case is not considered for flash initiation.

In experiments characterized by these conditions the species influencing the laser output are F, H_2, HF, and H. The effect of the fluorine precursor molecules (SF_6, CF_3I) will be taken into account only in an approximate manner, as a buffer gas contributing only to rotational relaxation.

(iii) Translational temperature[47]: The pumping reaction, V–T, R–T, and other processes (e.g., electron impact) release heat into the reactive mixture and raise its temperature. In the absence of rotational equilibrium temperature rise plays only a secondary role. The final temperature in the lasing system can be shown to

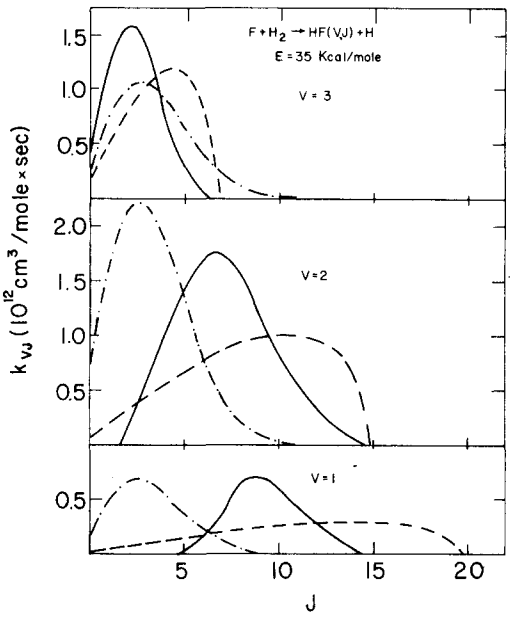

FIG. 3. Detailed rate constants of the pumping reaction (R.1), corresponding to three different vib–rotational distributions $P(V,J)$. $k_{VJ} \propto P(V,J)$. Solid curves represent the infrared chemiluminescence (IRC) data (Refs. 21 and 36), dashed curves correspond to the statistical model. The dot–dashed curves are thermal rotational distribution. The area under each curve is proportional to $P(V)$.

range between 400 and 600 °K; it is lower in the presence of a buffer gas. Since the temperature dependence of most of the relevant rate constants in this range is weak (or not accurately known), we have used a constant value of T (mostly 500 °K) in all computations. The use of $T = 300$ °K for $\Delta\nu_D$ is to correctly describe the threshold behavior, i.e., when T is still low. The subsequent change in $\Delta\nu_D$ is minor.

B. Pumping

The pumping reaction (R. 1), is highly exothermic: $E \sim 35$ kcal/mole for $T = 300$–500 °K. This energy suffices to populate all levels of HF below $(V,J) = 0, 23)$, $(1, 19)$, $(2, 14)$, and $(3, 6)$, Fig. 3.

The pumping term in (1) is given, in obvious notation, by

$$P_{VJ}(t) = k(-VJ)N_F(t)N_{HF}(t) - k(VJ-)N_H(t)N_{VJ}(t) \ . \quad (11)$$

The minor contribution of the second term in (11) was treated in an approximate manner.[32] The ratio between the detailed and total rate constants of the pumping reaction defines the product state distribution

$$P(V,J) = k(-VJ)\left(\sum_{VJ} k(-VJ)\right)^{-1} = k(-VJ)/k \ , \quad (12)$$

$$P(V,J) = P(V)P(J|V) \ , \quad (13)$$

$$\sum_{VJ} P(V,J) = \sum_{V} P(V) = \sum_{J} P(J|V) = 1 \ . \quad (14)$$

Here $P(V)$ and $P(J|V)$ are the initial vibrational and rotational (conditional within V) distributions in (R. 1).

The numerical values of the total[33] and detailed reactive rate constants (and those corresponding to relaxation processes, Table I) used in the modeling are collected in Table II. Three kinds of $P(VJ)$, which differ mainly with respect to the rotational distribution $P(J|V)$, were employed in the calculations, Fig. 3.

(a) IRC: The distribution measured by Polyani and Woodall[21] in the infrared chemiluminescence (IRC) method. Similar results for $P(V)$ were obtained by other authors using various techniques (IRC,[34–36] chemical lasers,[31,37] molecular beam[38]; classical trajectory[23–25,39–41] and collinear quantal[42] calculations). Since according to the IRC's $P(J|V)$ high J levels are not populated (compare Figs. 1 and 3), we test another initial distribution.

(b) "Statistical": The vibrational distribution is given by[31,43–45]

$$P(V) = P_0(V)\exp(-\lambda_\nu E_v/E)/Q \ ,$$
$$P_0(V) = B_v^{-1}(E - E_v)^{3/2}\left(\sum_v B_v^{-1}(E - E_v)^{3/2}\right)^{-1} \ . \quad (15)$$

Here λ_ν is a (vibrational temperature) parameter independent of V, Q is a normalization factor (partition function), and $P_0(V)$ a statistical ("prior") distribution,[43–46] where B_v is the rotational constant. Equation (15) describes[31,43] the experimental $P(V)$ with $E = 34.6$ kcal/mole ($T = 300$ °K) and $\lambda_\nu \simeq -6.5$. To account for the translational heating we have used slightly different values; $\lambda_\nu = -6.0$ and $E = 35.0$. This choice is based on the finding[37] that, in (R. 1), $\langle f_v \rangle = \langle E_v/E \rangle$ decreases with T ($-\lambda_\nu$ is a decreasing function of $\langle f_v \rangle$). As a representative distribution which (like some[23–25] but not all classical trajectory studies[41]) assigns nonvanishing probabilities to all rotational levels below the energy limit, we use the statistical (prior) function[14,22]

$$P(J|V) = (2J+1)[E - E_v - E_J(V)]^{1/2}/Q_R \ , \quad (16)$$

where Q_R is a normalization factor and $E_J(V) = hcB_vJ(J+1)$. Equation (16) corresponds to equipartitioning of nonvibrational energy[22]: $\langle f_R \rangle$; $\langle f_T \rangle = 2:3$.

(c) Thermal: $P(V)$ is the same as in (a), but $P(J|V)$ is a Boltzmann distribution at ($T = 500$ °K). This distri-

TABLE I. Pumping and relaxation in the $F + H_2$ laser.

I.	Initiation (a) Discharge $(SF_6 + e^-)$ (b) Flash $(CF_3I + h\nu)$	
II.	Pumping: $F + H_2 \rightleftarrows HF(VJ) + F$	(R.1)
III.	R–R, T transfer: $HF(VJ) + M \rightleftarrows HF(V,J') + M$	(R.2)
	$M = HF$, H_2, F, H, $SF_6(CH_3I)$, Ar	
IV.	V–R, T transfer: $HF(V,J) + M \rightleftarrows HF(V-1,J) + M$	(R.3)
	$M = H$, (H_2, SF_6, Ar)	
	$HF(V,J) + F \rightleftarrows HF(V-1,J') + F$	(R.4)
	$HF(V,J) + HF(V_1,J_1) \rightleftarrows HF(V',J') + HF(V_1',J_1')$	(R.5)
V.	V–V transfer:	
	$HF(V,J) + HF(V'J') \rightleftarrows HF(V\pm1,J) + HF(V'\mp1,J')$	(R.6)
	$HF(V,J) + H_2(0) \rightleftarrows HF(V-1,J) + H_2(1)$	(R.7)

TABLE II. Absolute values and VJ dependences of rate constants used in the modeling in units of $cm^3/mole \cdot sec$.

I. Pumping $F + H_2 \rightleftarrows HF(V, J) + H$

$k(\rightarrow V, J) = k\, P(V)P(J|V)$, $k = 2\times10^{13}$

a. IRC $P(V=0,1,2,3) = 0,\ 0.17,\ 0.56,\ 0.27$; $\langle f_v\rangle = 0.66$ $\langle f_R\rangle = 0.08$

b. Statistical $P(V=0,1,2,3) = 0,\ 0.19,\ 0.53,\ 0.28$; $\langle f_v\rangle = 0.63$ $\langle f_R\rangle = 0.15$

c. Thermal $P(V=0,1,2,3) = 0,\ 0.17,\ 0.56,\ 0.27$; $\langle f_v\rangle = 0.66$ $\langle f_R\rangle = 0.03$

For $k(V, J\rightarrow)$ and $P(J|V)$ see text and Fig. 3.

II. R–R, T $HF(V, J) + M \rightleftarrows HF(V, J') + M$

$k(J \rightarrow J' < J) = \bar{Z}\bar{N}(2J'+1)\exp[-C(E_J - E_{J'})]\cdot\bar{Z} = 1.8\times10^{14}$, $\bar{N} = 0.3$, $C = 8.5\times10^{-3}\ cm^{-1}$

$(2J'+1)k(J' \rightarrow J) = (2J+1)k(J \rightarrow J')\exp[(-E_J - E_{J'})/kT]$; $\Delta J = 0, 1, 2, \cdots$

III. V–R, T (i) $HF(V, J) + H \rightleftarrows HF(V-1, J) + H$

$k(V, J \rightarrow V-1, J) = k(V \rightarrow V-1) = P_v k(1 \rightarrow 0)$; $k(1 \rightarrow 0) = 3\times10^{12}$

$P_0; P_1; P_2 = 1;\ 5;\ 7.3$; $k(V-1 \rightarrow V) = k(V \rightarrow V-1)\exp(-\Delta E_v/kT)$.

(ii) $HF(V, J) + F \rightleftarrows HF(V-1, J') + F$

$k(V, J\ V-1, J') = \delta_{J', J+\Delta J} F(J) V k(1 \rightarrow 0)$; $k(1 \rightarrow 0) = 1.5\times10^{12}$

$F(J) = 1 + 0.1J$, $\Delta J = [(J+\frac{1}{2})^2 + 2\omega/3B]^{1/2} - (J+\frac{1}{2})$, Table III

$k(V-1, J+\Delta J \rightarrow V, J) = [(2J+1)/(2J+2\Delta J+1)]\exp(-\Delta E_{VJ}/kT)$

(iii) $HF(V, J) + HF(V_1, J_1) \rightleftarrows HF(V-1, J') + HF(V_1', J_1')$

$k(V, J, V_1, J_1 \rightarrow V-1, J', V_1, J_1'; T_t) = V\delta_{J', J+\Delta J}\delta_{J_1', J_1+\Delta J} k_{10}(J, J_1 \rightarrow; T_t)$

$k_{10}(J, J_1 \rightarrow) = k_{10}(\hat{J} \rightarrow) = k_{10}^R(\hat{T}) + k_{10}^t(\hat{T}) = \alpha(\hat{T})k_{10}(\hat{T}) + [1 - \alpha(500)]k_{10}(\hat{T})$

$= \alpha(\hat{T})k_{10}(\hat{T}) + 1.1\times10^{11}$; $k_{10}(T) = 1.7\times10^6 T^{1.77} + 1.1\times10^{13}T^{-0.4} = k_{10}^{exp}(T)$,

where $\Delta J = [(J+\frac{1}{2})^2 + \beta\omega/2B]^{1/2} - (J+\frac{1}{2})$, similarly for ΔJ, Table III

$\hat{J} \equiv \max\{J, J_1\}$, $\hat{T} = (2\hat{J}+1)^2 hcB/2k$, $\beta = 0.9$, $T_t = 500\,^\circ K$

$\alpha(\hat{T} = 400, 1000, 2000, 3000, 4000\,^\circ K) = 0.96,\ 0.82,\ 0.69,\ 0.61,\ 0.57$

$k_{01}(J', J_1' \rightarrow J_1;\ T_t) = (g_J g_{J_1}/g_{J'} g_{J_1'})\exp(-\Delta E_t/kT_t) k_{10}(J, J_1 \rightarrow J', J_1';\ T_t)$

$g_J = 2J+1$; $\Delta E_t = (1-\beta)hc\omega \simeq 1.1$

IV. V–V (i) $HF(V, J) + HF(V', J') \rightleftarrows HF(V \pm 1, J) + HF(V' \mp 1, J')$

$\Delta J = \Delta J' = 0$. Numerical values of $k(V, V' \rightarrow V \pm 1, V' \mp 1)$, Fig. 4.

(ii) $HF(V) + H_2(0) \rightleftarrows HF(V-1) + H_2(1)$, $\Delta E \simeq 250\ cm^{-1}$

$k(V, 0 \rightarrow V-1, 1) = v\ k(1, 0 \rightarrow 0, 1) = k(V-1, 1 \rightarrow V, 0)\exp(-\Delta E/kT)$

$k(0, 1 \rightarrow 1, 0) = 1\times10^{12}\ k(1, 0 \rightarrow 0, 1) = 5.7\times10^{11}$

bution serves for comparison with the nonequilibrium distributions above.

C. Relaxation

In this section we present some of the considerations leading to the choice of rate constants listed in Table II, and provide some details which cannot be given there. [More details are given in Ref. 19(b), general background in Refs. 48 and 49.] The V, J dependence of typical rate constants is shown in Fig. 4. The collisional loss terms in (1) will be discussed in accordance with the symbolic decomposition

TABLE III. "Selection rules" for V–R, T transfer.

J	ΔJ HF–F	ΔJ HF–HF	J	ΔJ HF–F	ΔJ HF–HF
0	11	9	10	5	3
1	10	8	11	4	3
2	9	7	12	4	3
3	8	6	13	4	3
4	7	6	14	4	2
5	7	5	15	3	2
6	6	5	16	3	2
7	6	4	17	3	2
8	5	4	18	3	2
9	5	3	19	3	2

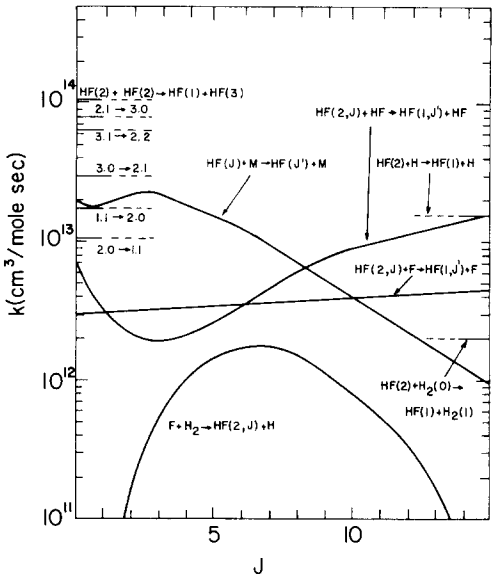

FIG. 4. J dependence of pumping and relaxation rate constants for HF($V=2, J$) molecules. Truncated horizontal lines correspond to J-independent rate constants. The curve HF(J) + M → HF(J') + M represents $k(J\rightarrow)$, the total $R-T$ rate constant out of J. Reversed $V-V$ rate constants, indicated on the left ordinate, have been calculated from the forward rate constants using $T=500\,^\circ$K in the detailed balance relation.

$$L_{VJ} = L_{VJ}^{R-R,T} + L_{VJ}^{V-R,T} + L_{VJ}^{V-V} \quad . \tag{17}$$

1. R-R,T transfer

A model for rotational energy transfer which accounts for the rotational relaxation in hydrogen halides has been proposed by Polanyi and Woodall[26] and (modified) by Ding and Polanyi.[27] The version of the model given in Table II is based on the "exponential gap law" for the deactivation ($J\rightarrow J'<J$) probability[50]

$$P(J\rightarrow J') = N(2J'+1)\exp[-C(E_J - E_{J'})] \,, \tag{18}$$

where N and C are parameters which we take as temperature independent. [$P(J\rightarrow J')$ is slightly V dependent through $E_J(V)$.] For large J values (which are of interest here) the probability of $R-T$ transfer is dominated by the rapidly decreasing exponential factor, Fig. 4. Since this trend was confirmed in various molecular systems,[51–53] we use (18) for all collision partners. Moreover, C and the product ZN where Z is the hard sphere collision frequency[54] are taken to be independent of M [$k(J\rightarrow J') = ZP(J\rightarrow J')$]. Using $\langle Z_{\rm rot}\rangle = 1/\langle P(2-)\rangle = 1/7$ (Refs. 55, 56), the value of C was optimized according to the procedure suggested in Ref. 26; the doubly peaked rotational relaxation patterns[21] were almost exactly reproduced.[57]

The net loss of HF(VJ) molecules by $R-R$, T transfer is

$$L_{VJ}^{R-R,T} = \left[k_v(J\rightarrow)N_{VJ} - \sum_{J'} k_V(J'\rightarrow J)N_{VJ'}\right]M, \tag{19}$$

where $M = N_{H_2}(0) + N_F(0) + N_{SF_6}(0) + N_{Ar}$ N_{Ar} represents any buffer gas.

2. V-R,T transfer

The present modeling requires detailed rate constants of the form $k(VJ\rightarrow V'J';T)$. However, the measured quantities are usually their thermal averages $k(v\rightarrow;T)$. Thus, approximations (sometimes inevitably drastic) based on theoretical inferences and guided by the need for computational convenience were employed by us in deriving the explicit expressions in Table II. Our intention is that at least the major effects of each process on the laser output will be properly represented.

(i) HF–H collisions: The numbers in Table II are based on the upper limits to $k(v\rightarrow;T)$ of (R. 3) reported by Kwok and Wilkins[58] (extrapolated to 500 °K on the basis of trajectory studies[59–61]). More recent studies[62] indicate that (R. 3) is 1–2 orders of magnitude slower (see, however, Sec. III. A.3). The harmonicity assumption [$k(V\rightarrow V-1) = vk(1\rightarrow 0)$, $\Delta V = \pm 1$], which somewhat contradicts the trajectory studies,[59–61] was made for simplicity. The sensitivity of the solutions of (1) and (2) to this assumption is low.[19b] Finally, the loss of HF(VJ) molecules due to (R. 3) is

$$L_{VJ}^{V-T}(\text{HF–H}) = [k(V\rightarrow V-1)N_{VJ} - k(V-1\rightarrow V)N_{V-1,J} - k(V+1\rightarrow V)N_{V+1,J} + k(V\rightarrow V+1)N_{VJ}]N_H \,. \tag{20}$$

(ii) HF–F collisions: In the context of the present work the role of (R. 4) is more interesting than that of (R. 3) since its major effect is $V-R$ transfer which may serve, at least in principle, as a secondary pumping mechanism of high rotational levels.[63] The data in Table II are based on shock tube measurements[64,65] at high temperatures and theoretical studies at low temperatures.[66–69] The assumption of harmonic behavior in this case is reasonable.[67–69] The $F(J)$ factor accounts for the increase in $V\rightarrow R$ probability with J.[70] The $\delta_{J',J+\Delta J}$ "selection rule" corresponds to $\langle E_{\rm rot}\rangle \simeq (2/3)\langle -\Delta E_{\rm vib}\rangle$[67,68] and, moreover, to concentrating all the vibrational energy transferred to rotation in a single final J. This "one-to-one" correspondence which was assumed to reduce the computational effort seems reasonable because (1) The rotational distribution in $V-1$ resulting from a superposition of one to one transitions from V cannot be significantly different from that resulting from a one to many scheme. (2) $R-R$, T transfer tends to smooth local irregularities in the rotational distributions. The expression for $L_{VJ}^{V-R,T}$(HF–F) is straightforward but cumbersome and will therefore be omitted.

(iii) HF–HF collisions: The mechanism of $V-R$, T transfer in HF–HF collisions is by far more complex than for HF–H, HF–F. Nevertheless, the amount of information on HF, DF self-relaxation[71] is considerably larger.[48,49] The main findings and interpretations on which the rate constants of Table II and Fig. 4 were formulated are (1) HF($V=1$) relaxation is appreciably faster than in any other HX–HX system. In particular (except at very high temperatures), it is faster than DF–DF relaxation. (2) The Landau–Teller plot of $P\tau$ is nonlinear and displays a wide maximum between $T = 600$–$1000\,^\circ$K. The high relaxation rates and the non-

TABLE IV. Effects of kinetic processes on laser performance.

$P(V,J)$ initial conditions	Relaxation scheme	τ_{th} (μsec)	τ_q[a] (μsec)	$\hat{P}(J)$[b] $2\rightarrow1$	ϕ_q[c]	ϕ_t[d]	Q[e]	$\frac{Q_{3\rightarrow2}}{Q_{2\rightarrow1}}$[f]	$\frac{Q_{1\rightarrow0}}{Q_{2\rightarrow1}}$	$P(V)$, $V=0$	(%) 1	$t=\tau_q$ 2	3
IRC	No Rel.[g]	0.6	14	5	1.0	0.8	4.6	0.37	0.71	33	31	27	9
discharge	$R-T$	0.6	15	7	1.0	0.8	4.7	0.37	0.72	34	31	26	9
$F:H_2=1:10$	$R-T+V-V$	0.6	15	4	1.0	0.8	4.5	0.41	0.70	34	30	25	11
	High $R-T$[h]	0.7	(30)	7	1.4	1.4	8.3	0.31	0.89	59	25	11	5
	All[i]	0.6	14	4	0.9	0.7	4.2	0.40	0.72	35	31	26	11
IRC	No Rel.	0.2	(30)	5	1.0	0.8	39.4	0.34	0.73	35	31	27	7
discharge	$R-T$	0.2	(30)	4	1.0	0.8	42.5	0.37	0.71	38	30	23	9
$F:H_2=5:6$	$R-T+M$[j]	0.2	(30)	5	1.1	0.9	45.5	0.34	0.80	42	29	20	9
	$V-V$	0.2	14	5	0.6	0.4	20.3	0.46	0.63	34	31	26	9
	$R-T+V-V$	0.2	17	4	0.6	0.4	21.6	0.47	0.60	48	24	17	11
	$V-R,T$	0.2	(22)	4	0.6	0.5	26.9	0.37	1.01	35	32	25	8
	High $R-T$	0.2	(30)	8	1.3	1.1	55.5	0.30	0.92	63	24	9	4
	All	0.2	13	4	0.6	0.4	19.4	0.46	0.68	41	28	20	11
Thermal	No Rel.	0.6	15	4	0.9	0.7	4.4	0.26	0.75	34	29	22	15
discharge	$R-T$	0.5	18	4	0.8	0.7	4.3	0.27	0.77	38	28	20	14
$F:H_2=1:10$	High $R-T$	0.6	(30)	7	1.4	1.4	8.5	0.32	0.88	59	24	11	6
IRC	No Rel.[g]	4.0	21	5	1.0	0.6	3.8	0.37	0.71	33	31	27	9
flash	High $R-T$[h]	3.5	(40)	7	1.4	1.3	7.9	0.31	0.88	58	25	11	6
$F:H_2=1:10$	All[i]	4.0	24	4	0.9	0.6	3.7	0.37	0.72	34	31	26	9
Thermal flash, 1:10	High $R-T$	4.0	(40)	7	1.4	1.3	8.0	0.32	0.88	58	25	11	6
Statistical	No Rel.	0.8	11	7	0.9	0.7	4.25	0.41	0.73	33	31	26	10
discharge	$R-T$	0.8	11	6	1.0	0.7	4.3	0.41	0.74	34	31	25	10
$F:H_2=1:10$	$V-V$	0.8	9	7	0.9	0.6	3.6	0.43	0.72	32	31	26	11
	High $R-T$	0.8	(30)	7	1.4	1.4	8.4	0.36	0.92	59	25	11	5
	All	0.8	10	7	0.9	0.6	3.6	0.42	0.73	32	31	26	11
Statistical	No Rel.	0.3	28	7	0.9	0.7	38.2	0.36	0.76	35	31	25	9
discharge	$R-T$	0.3	30	5	1.0	0.8	41.7	0.37	0.78	38	31	23	8
$F:H_2=5:6$	$V-V$	0.3	12	7	0.6	0.4	20.0	0.50	0.65	38	27	22	13
	$V-V$ (low)[k]	0.3	20	7	0.8	0.6	31.5	0.42	0.73	34	30	25	11
	All	0.3	12	6	0.6	0.4	18.6	0.48	0.71	41	28	20	11
	All (low $V-V$)	0.3	25	6	0.7	0.6	27.8	0.39	0.97	41	33	9	7

[a]The quenching times were determined by the (somewhat arbitrary) requirement that at $t=\tau_q$, all q_{VJ}'s are less than 10^{-13} mole·photon/cm^3. Numbers in parentheses correspond to long tail pulses. Practically, at $t \gtrsim 30$ μsec the reaction is already completed, Fig. 2.

[b]$\hat{P}_{2\rightarrow1}(J)$ is the most intense transition (it always occurs in the $V=2\rightarrow1$ band).

[c]Photon yield; photons per HF molecule at τ_q.

[d]Photon yield; photons per HF molecule at $t\rightarrow\infty$.

[e]Total pulse energy in units of 10^{-10} mole·photon/cm^3.

[f]$Q_{V\rightarrow V-1}/Q_{V-1\rightarrow V-2}$ is the ratio between band intensities.

[g]No rel. means no relaxation processes included.

[h]High $R-T$ corresponds to $M=3\times10^{-6}$ mole/cm^3 in (19).

[i]All means a full run, all relaxation processes included.

[j]Here $M=5.2\times10^{-8}$ mole/cm^3, 3 times larger than in the normal $R-T$.

[k]Low $V-V$ means $V-V$ rate constant for HF–HF taken smaller by 1 order of magnitude.

linearity of the LT curves at low temperatures are attributed to the strong dipole–dipole interactions.[49,72–74] The isotopic effect (DF slower than HF) can be explained as the result of strongly preferred $V-R$ (over $V-T$) transfer.[73–76] The maximum in the L, T plot is explained as the net result of the "short range $V-R$, T" and the "long range $V-R$" mechanisms governing the relaxation at high and low temperatures, respectively. At very high T the $V-T$ mechanism becomes important and DF relaxes faster than HF.[75,76]

We now briefly outline some of the specific approximations and assumptions leading to the expresssions in Table II. (1) The rate constants are linear in V and independent of V_1. $\Delta V=\pm1$. (2) The major mechanism is $V\rightarrow R$. A fraction β of the vibrational energy transfer $hc\omega$ is released as rotational energy. Inter- and intramolecular $V\rightarrow R$ transfer have the same probability ($\frac{1}{2}\beta hc\omega$ for each molecule). To each J, J_1 a single $J'=J+\Delta J$, $J_1'=J_1+\Delta J_1$ combination ["selection rule," see (ii) above] corresponds. Large ΔJ jumps and significant J dependence, Table IV, Fig. 4, were indicated by several authors[78,79] (see, however, Ref. 80), on the basis of experiment and theory.[81,82] (3) The dependence of the rate constants on J, J_1 is governed by $\hat{J}=\max\{J,J_1\}=\frac{1}{2}[J+J_1)+|J-J_1|]\simeq I\bar{\omega}/h$, where $\bar{\omega}$ is the average rela-

tive rotational velocity of the colliding pair.[63d] (4) The temperature dependence of $k_{10}^{exp}(T)$ is dominated by the rotational motion. To determine $k_{10}(\hat{J}\rightarrow)$ we thus consider $k_{10}(\hat{T})$, where $\hat{J}$ is the most probable J at temperature $\hat{T}$.[77] The (small) contribution of the translational motion (with constant T_t) is accounted for by a correction factor $\alpha(\hat{T})$ suggested by Shin.[74] (5) Note that because $\exp(-\Delta E_t/kT_t)$ is small, activation and deactivation rates are not much different.

Writing down L_{VJ}^{V-RT}(HF–HF) is a straightforward but tedious task and will therefore be left out.

3. V–V transfer

Owing to their near resonant character, $V-V$ processes are generally fast and do not involve large ΔJ changes.[81,82] In the absence of rotational equilibrium, $V-V$ exchange can affect the rotational populations.

(i) HF–HF collisions: Rate constants attributed to the process $HF(V)+HF(0)\rightleftarrows HF(V-1)+HF(1)$ were measured by Osgood, Sacket, and Javan[83] for $V=2,3,4$. Similar results and a T^{-1} dependence (for DF) were reported by Bott[84,85] (for $V=2$). We adopted the T^{-1} dependence to extrapolate the room temperature measurements of Ref. 83 to $T=500\,^{\circ}K$. The values in Table II and Fig. 4 correspond to gas kinetic transition probabilities of ~ 0.5. These values are an order of magnitude larger than the $V-R, T$ rates, (R. 5). (Some calculations were carried out with lower values—Sec. III.) The excitation rates are higher than the de-excitation rates owing to the large anharmonicity of HF. As proposed in Ref. 83, the "asymmetry" of the $V-V$ rates[86,87] may enhance the lasing from $V=3$.

We assume that, in (R. 6), $\Delta J=0$ and ignore $V\geq 4$ (see Sec. III). $k(3,1\rightarrow 2,2)$ was estimated from $k(2,0\rightarrow 1,1)$ and $k(3,0\rightarrow 1,1)$ using $k(V,V'\rightarrow V-1,V'+1)=V(V'+1)k(1,0\rightarrow 0,1)$. Finally,

$$L_{VJ}^{V-V}(\mathrm{HF-HF})=\sum_{V_1=V\pm 1}\sum_{V'=0}^{3}[k(v,V'\rightarrow V_1,V_1')N_v\cdot N_{VJ}-k(V_1,V_1'\rightarrow V,V')N_{V_1'}N_{V_1J}]\,, \tag{21}$$

where some of the rate constants are identically zero.[88]

(ii) HF–H_2 collisions: H_2 molecules can deactivate HF via near resonant $V-V$ transfer or via $V-R, T$ transfer. Since (R. 7) is a relatively slow process,[87] it is mainly influential when $[H_2]$ is large, i.e., in the F : H_2 = 1 : 10 case. Only $H_2(V=0,1)$, ($[H_2(0)]\approx[H_2]\gg[H_2(1)]$) are considered in the modeling. The rate constants of (R. 7) were measured by several authors, e.g., Refs. 80, 89. The expression for $L_{VJ}^{V-V,T}(\mathrm{HF-H_2})$ is obvious.

III. RESULTS AND DISCUSSION

The laser rate equations (1) and (2) were solved for several initial conditions (Sec. II), with various "kinetic schemes" for every initial condition. A kinetic scheme is specified by the product state distribution in the pumping reaction (IRC, statistical, or thermal) and by a certain combination of relaxation processes, e.g., "no relaxation," $R-T$, $R-T+V-V$, or high $R-T$. No relaxation means $L_{VJ}\equiv 0$ in (1), (2); $R-T$ means that only pumping, stimulated emission, and rotational relaxation are considered in the calculation, etc. The rate equations were solved using a fourth order Runga–Kutta–Gill integrator.

The solutions of the rate equations provide the time evolution of the vib–rotational populations, $N_{VJ}(t)$, and the photon densities, $q_{VJ}(t)$. The profile of each $P_{V\rightarrow V-1}(J)$ laser pulse is reflected by the corresponding $q_{VJ}(t)$.[90] The integrated output energy I_{VJ}, or Q_{VJ}, obtains from $q_{VJ}(t)$ according to (4). The q_{VJ}'s are oscillatory functions (strongly, just after threshold) whose fine structure between τ_{th} and τ_q is very sensitive to variations in the initial conditions or in the kinetic scheme. The integrated output energies, being averaged quantities, are less sensitive to such variations and reflect only the major effects of each kinetic process. Thus, the results will be generally presented in terms of the Q_{VJ}'s.

The specific effect of a given kinetic process on the laser output may be amplified, surpressed, or unaffected, depending on the initial conditions and the strength of the other kinetic factors. Still, as a guideline for a systematic analysis of the results presented in Figs. 5–18 and in Tables IV and V, a separate discussion of the major effects of each kinetic factor seems appropriate.

A. Effects of rate processes

1. Effect of P(V,J)

The spectral composition of the laser outputs resulting from the IRC and the statistical distributions (for the initial condition discharge 1 : 10) are shown in Figs. 5 and 6, respectively. Figures 7 and 8 illustrate the results for F : H_2 = 5 : 6.

These figures clearly demonstrate that, except for the case of high $R-T$, the output pattern is, to a large extent, a reflection of the pumping function (the product state distribution). This is particularly so in the F : H_2 = 1 : 10 case, where the energy transfer processes have only a minor effect on the output.

As an illustrative example consider the statistical distribution, Fig. 6. Comparison with Fig. 3 indicates that Q_{3J}, the laser energy radiated in the $P_{3\rightarrow 2}(J)$ band, is very similar in shape to $P(J/V=3)$. Since radiational cascades do not affect $V=3$, this means that on the average, the gain $\alpha_{3,J}$ is proportional to $P(J/3)$. The gain coefficient is given by

$$\alpha_{VJ}\equiv\alpha_{V,J-1\rightarrow V-1,J}=c\sigma_{V,J-1\rightarrow V-1,J}\left(N_{V,J-1}-\frac{(2J-1)}{(2J+1)}N_{V-1,J}\right). \tag{22}$$

If relaxation processes are not effective, as in the present case, then at least in the early stages of the pulse $N_{3J}\propto k_1(3,J)\propto P(J/3)$ and $N_{2,J\leq 7}<[(2J+1)/(2J-1)]N_{3,J}$. Since σ is almost independent of J, it follows that $Q_{3,J}$ will be roughly proportional to $P(J/3)$. The lasing in the $V=3\rightarrow 2$ band populates the low J states in $V=2$ and leads to a peak of $Q_{2,J}$ around $J=6$. The peak at $J=12$ results from the chemical pumping into $V=2$, Fig. 3. The radiative cascade is also reflected in the $V=1\rightarrow 0$

TABLE V. Threshold and quenching times. $\tau_{th}-\tau_q$ (μsec).[a]

		IRC 1:10 discharge			Statistical 1:10 discharge		IRC 1:10 flash	
		No Rel.	$R-T$	High $R-T$	$R-T$	High $R-T$	All	High $R-T$
$P_{3\to2}$	(2)	0.6–12	0.6–12		1.2–1.8		4.5–20	
	3	0.6–13	0.6–13	1.2–2	0.9–7	1.1–1.8	4.0–21	
	4	0.9–10	0.9–10	1.1–4	0.8–9	1.0–4	4.5–13	5–10
	5			3.0–7	0.8–9	1.2–6		7–15
	6			6.0–13	0.9–8	6.0–13		13–24
	7			12–22	1.3–3	1.2–22		23–34
$P_{2\to1}$	(2)							
	3	1.0–10	0.9–13	0.7–1.7	1.4–7	0.8–1.7	5.0–19	4–6
	4	0.8–13	0.8–15	0.7–5	1.1–9	0.8–1.4	4.5–24	3.5–8
	5	0.7–13	0.7–13	0.7–8	1.0–10	0.8–8	4.5–21	5–12
	6	0.6–13	0.6–12	0.8–9	0.9–11	0.9–9	4.5–18	7–21
	7	0.6–12	0.6–12	1.0–22	0.9–11	1.1–22	4.0–18	9–30
	8	0.7–12	0.7–11	1.3–31	0.9–7	1.1–31	4.5–16	13–40
	9	0.7–11	0.7–10	1.8–5	0.8–7	1.2–6	4.5–14	
	10	0.9–8	0.9–8		0.8–7	1.2–1.5	5.0–7	
	11	0.9–5	1.1–4		0.8–7	1.2–1.6	6.0–7	
	12		1.5–3		0.8–7	1.3–1.6		
$P_{1\to0}$	(3)			1.1–2		1.2–2		6–7
	4			1.1–3	3.0–4	1.3–3		5–8
	5	1.4–6	1.4–9	1.1–4	1.8–7	1.3–4	6.5–10	6–11
	6	1.3–9	1.3–9	1.3–8	1.6–7	1.4–7	6.5–10	8–15
	7	1.3–10	1.3–9	1.7–15	1.5–7	1.9–15	6.0–9	10–25
	8	1.1–10	1.1–9	3.0–31	1.4–6	3.0–31	5.5–9	12–36
	9	1.0–10	1.0–10	5.0–25	1.6–5	5.0–25	5.5–15	21–35
	10	1.0–9	1.0–9		1.5–5		5.5–13	
	11	1.2–5	1.2–7		1.4–5		6.0–9	
	12	1.3–4	1.4–5		1.4–5		6.5–8	
	13	1.4–3	1.8–4		1.4–5			
	14				1.4–5			

[a]See footnote a in Table IV.

band; the peaks at $J=6$ and 13 result from $V=2\to1$ transitions, while the "shoulder" around $J=18$ is due to the chemical pumping $-P(J/1)$. In the IRC 1:10 case, Fig. 5, the humps in Q_{VJ} resulting from the radiative cascades are not so clearly separated because of the larger overlap between the original rotational distributions, Fig. 3.

As distinguished from the individual Q_{VJ}'s, the total energy radiated in the $V\to V-1$ band

$$Q_{V\to V-1}=Q_V=\sum_J Q_{VJ} \qquad V=1,2,3 \tag{23}$$

is not very sensitive to the initial rotational distribution, Table IV. This is because the $Q_{V\to V-1}$'s are primarily determined by the vibrational distributions; the IRC and the statistical $P(V)$'s are almost the same. The thermal distribution, Fig. 3, deviates from this rule. In this case the rotational distributions in different vibrational manifolds overlap, and since $P(V=3)<P(V=2)$ lasing in the $V=3\to2$ band occurs only because of partial inversion.[5–10] Consequently, in the (hypothetical) case of thermal $P(V,J)$ with no relaxation (or with "normal" rotational relaxation), the ratio $Q_{3\to2}:Q_{2\to1}$ is smaller than for IRC or statistical $P(V,J)$'s, Table IV.

2. *Rotational non-equilibrium and R-T transfer*

The effects of enhanced rotational relaxation on the spectral distribution and overall intensity of the laser pulse are clearly seen in Figs. 5–7 and Table IV. Comparison of the high $R-T$ curves in Figs. 5 and 6 indicates, as expected, that the fast rotational relaxation erases completely the memory of the initial product distribution. The IRC, statistical, and thermal initial distributions lead to the same output pattern (see also the data for ϕ, $Q_{V\to V}$, etc., in Table IV). Not shown in these figures are the different effects of low and high pressures on the finer details of the laser pulse, e.g., on τ_{th} and τ_q of specific transitions. Before considering these points in more detail, let us briefly outline the traditional description of chemical lasers in rotational equilibrium.[4–10]

In order that lasing in a certain vib–rotational transition be possible, the gain must exceed the threshold value $\alpha_{th}=c\sigma\Delta N_{th}=\tau^{-1}$, see Eq. (2). Since $\sigma_{V,J-1\to V-1,J}$ is almost independent of J [see, e.g., Refs. 4(j), 10] the relative gains are primarily determined by the population inversion, particularly so in the state of rotational equilibrium, where the effective populations $N_{VJ}/(2J+1)$ decrease exponentially with $J(J+1)$. In this case the necessary, P-branch, lasing condition, $\Delta N_{V,J-1\to V-1,}$.

>0, reads

$$\frac{N_V}{N_{V-1}} > \exp\left(\frac{-2hcB}{kT} J\right), \tag{24}$$

where, for simplicity, we employed the rigid rotor level scheme $E_J = hcBJ(J+1)$. In principle, lasing can simultaneously occur on all lines consistent with (24). However, this lasing criterion is only valid if rotational equilibrium prevails throughout all lasing stages, i.e., if rotational relaxation is instantaneous. (The term instantaneous is used here to mean that rotational relaxation is fast enough to smooth over any changes in the rotational distributions caused by other rate processes, e.g., to prevent "hole burning" by the stimulated emission.) Consequently, at every moment only one—the "highest gain"—transition can lase. In general, the highest gain transition corresponds to the lowest J, satisfying (24), say $J-1 \rightarrow J$. As a result of the lasing, N_V/N_{V-1} decreases until at some moment (24) is no longer fulfilled by the $J-1 \rightarrow J$ transition and the lasing is shifted to the subsequent highest gain transition $J \rightarrow J+1$, and so on. Throughout the J-shifting process

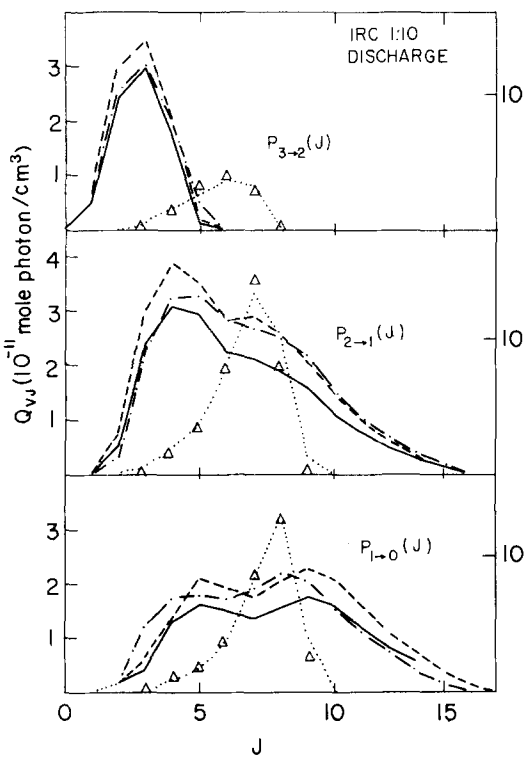

FIG. 5. Spectral distribution of the integrated output energy corresponding to initial IRC distribution, discharge initiation, and initial concentration ratio $F:H_2 = 1:10$. -·-·- represents the results when no relaxation processes are included in the rate equations (i.e., only pumping and radiation are considered). ---, $R-T$ transfer processes (due to H_2, HF, F, H, and fluorine precursor) included; $M = 1.26\times10^{-8}$ mole/cm^3, or $P \sim 0.5$ torr in Eq. (19). ——, All relaxation processes taken into account. The right-hand scale (units as on lhs) refers to the high $R-T$ results ($M = 3\times10^{-6}$ mole/cm^3, $P \sim 80$ torr. $V-V$ and $V-R, T$ processes disregarded). ·····, High $R-T$ with initial IRC distribution. Δ, High $R-T$ with initial thermal distribution. The two sets of high $R-T$ results show that enhanced rotational relaxation improves the efficiency and, as expected, erases the memory of the initial rotation distribution.

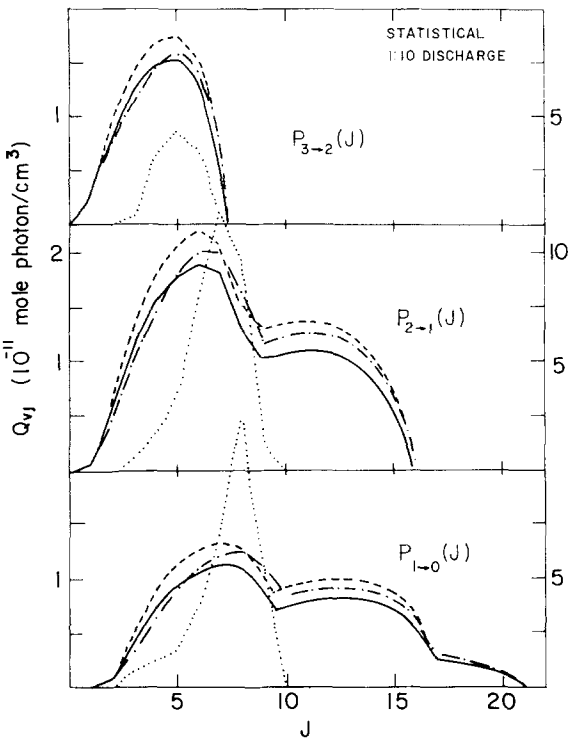

FIG. 6. Spectral distribution of integrated output energy corresponding to statistical initial distribution. -·-·-, No relaxation, ---, $R-T$, —— all relaxation processes included (left-hand scale). ·····, High $R-T$ (right-hand scale). Note that the high $R-T$ results coincide with those of the IRC distribution, Fig. 5.

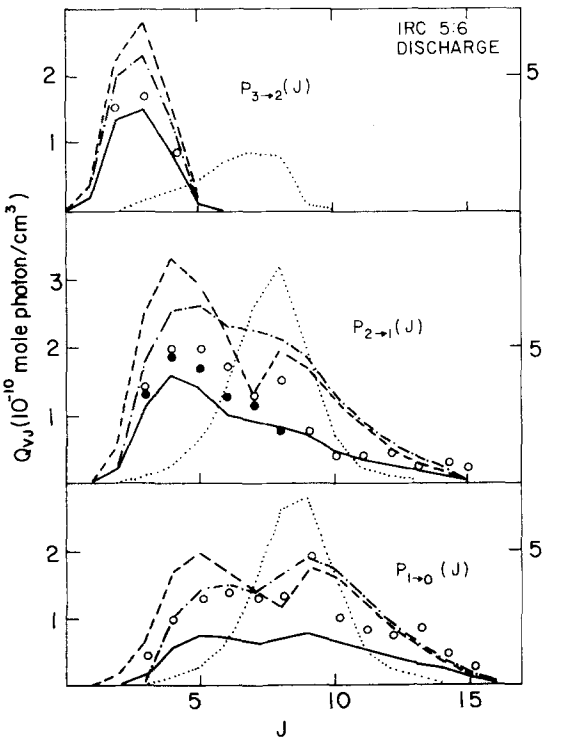

FIG. 7. Spectral distribution of integrated output energy, initial concentration ratio $F:H_2 = 5:6$. -·-·-, No relaxation. ---, $R-T$ ($M = 1.7\times10^{-8}$ mole/cm^3, $P \sim 0.5$ torr). ——, All relaxations; o correspond to the case when only $V-R, T$, relaxation is taken into account; ● similarly for $V-V+R-T$; where not indicated the solid circles almost coincide with the "All" curve. ···, High $R-T$ (right-hand scale).

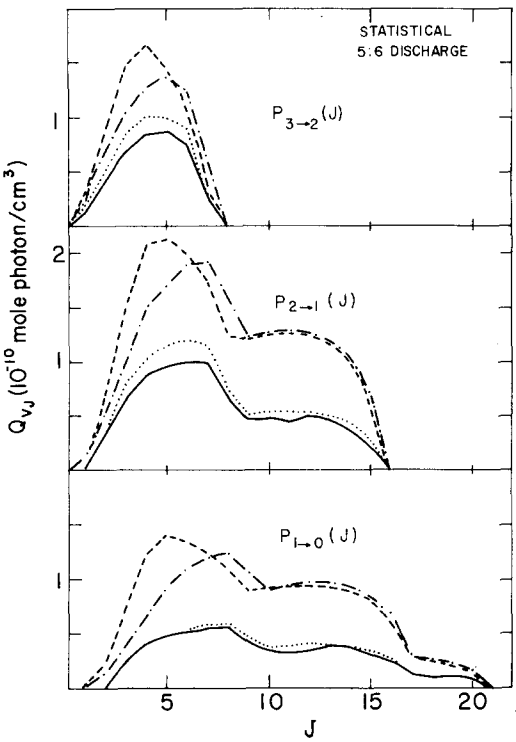

FIG. 8. Spectral distribution of integrated output energy. -·-·-, No relaxation; ---, $R-T$; ···, $R-T+V-V$; ——, all.

the fast rotational relaxation ensures rotational equilibrium; no hole is burnt in the rotational distribution of the upper vibrational level and no hump is created in the lower level. (This "funneling" mechanism[31,91] resembles lasing in homogeneously broadened spectral lines; the entire line profile—the analogue of the rotational distribution—is drained through the highest gain cavity mode). From (24) it is clear that J shifting can also result from a rise in T.[4-10] Considering, however, that to ensure rotational equilibrium the total pressure in the laser must be appreciable, the temperature rise (for example, due to the pumping reaction) cannot be significant.[31] Thus, the main cause for the J shift is

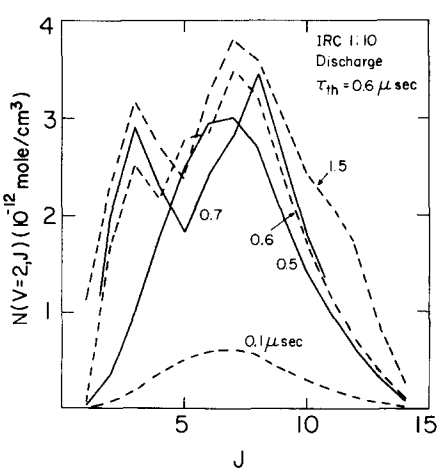

FIG. 9. Stages in the temporal evolution of the rotational distribution (in $V=2$) at low pressure. Numbers associated with each curve indicate time in microseconds.

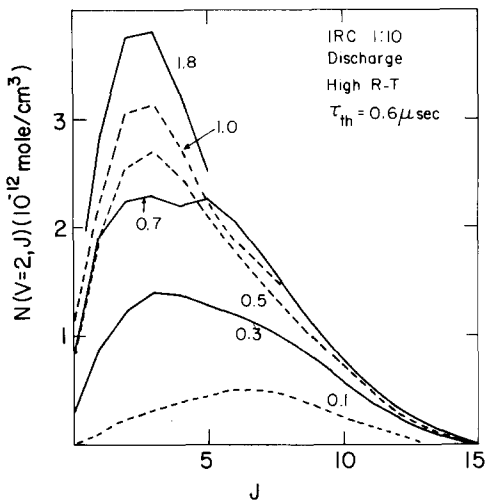

FIG. 10. Stages in the temporal evolution of the rotational distribution (in $V=2$) at high pressures. Numbers indicate time in microseconds.

the decrease in N_V/N_{V-1}. It should be mentioned that the qualitative description given above is mainly appropriate to the case of partial inversion ($N_V < N_{V-1}$); we shall see below that if $R-T$ transfer is fast, the major part of the laser energy is extracted from partially inverted populations.

Figures 9 and 10 illustrate some early stages in the temporal evolution of the rotational distribution of HF($V=2$) molecules. Figure 9 represents the situation when only F, H_2, HF, H, and fluorine percursor molecules are responsible for rotational relaxation, while Fig. 10 corresponds to the case where a buffer gas is added to the mixture to enhance rotational equilibrium. In the first case, Fig. 9, the relatively slow rotational relaxation does not affect the growth of N_{2J} due to the pumping, i.e., before threshold $N_{2J} \propto P(J/2)$—the rotational distribution in (R. 1), Fig. 3. The irregularities in N_{VJ} immediately after threshold ($t=0.6$ μsec), namely, the hump in $J=3$ and the dip in $J=6$, result from the start of lasing in $P_{3\to2}(3)$ and $P_{2\to1}(7)$, respectively. These two transitions are the first to reach threshold, Table V. N_{2J} remains irregular also after threshold, indicating that the $R-T$ transfer is slower than stimulated emission. The picture is entirely different in Fig. 10. Here the fast rotational relaxation ensures rotational equilibrium before threshold and maintains it afterwards. The truncation of N_{2J} at $J=2-4$ [$P_{2\to1}(3-5)$ lase first, Table V] is rapidly compensated by removal of molecules from higher rotational levels.

Figure 11 is the analog of Fig. 10 for the statistical rotational distribution. In this case, $R-T$ transfer is fast enough to suppress irregularities around the thermal peak ($J_{mp}=2-3$) but not to completely deplete the high, non-Boltzmann, levels. This is due to the exponentially decreasing rate of $R-T$ transfer at high rotational levels.

A simple estimate of the average number of collisions suffered by an HF molecule can indicate whether rotational equilibrium will be achieved before thresh-

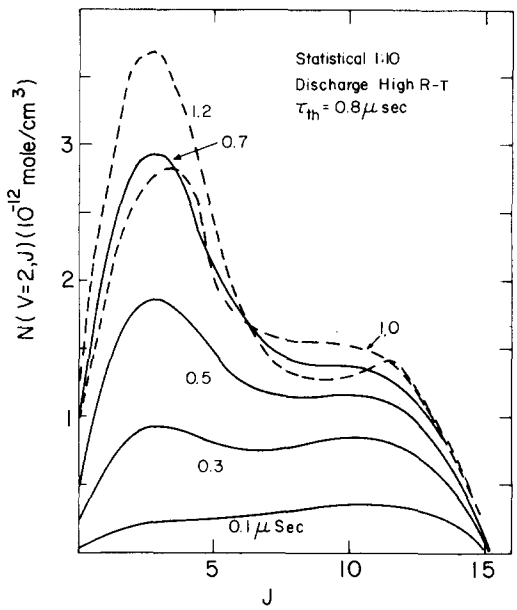

FIG. 11. Stages in the temporal evolution of the (initially "statistical," $V=2$) rotational distribution under conditions of enhanced rotational relaxation. The peak of $J \simeq 12$ is due to the primary distribution in the pumping reaction.

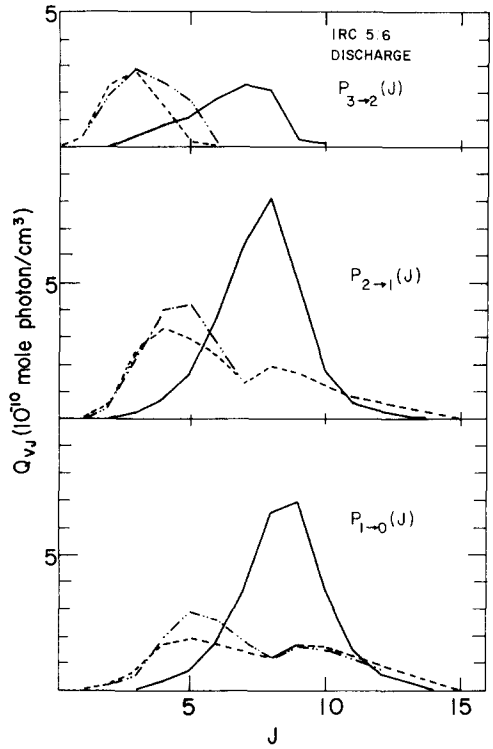

FIG. 13. Laser outputs at three different total pressures, ---, $P \sim 0.5$ torr; -·-·-, 1.5 torr; ——, 80 torr. The two low pressure results differ only at the low J values.

old. Using the values for $\bar{Z}$, M, $P(J\to)$ mentioned in Sec. II, one finds that for HF($J=2$) the number of effective (rotationally inelastic) collisions per 1 μsec is $\sim \frac{1}{2}$ in the low pressure case and ~100 in the high pressure case. For $J=12$—the peak in the statistical $P(J/2)$—the collision frequency is ~10 μsec^{-1} [$P(12\to)/P(2\to) \sim 1/10$, Fig. 4]. Thus, an HF($J=12$) molecule produced between $t=0$ and $\tau_{th}=0.8$ μsec suffers only ~4 collisions till threshold. Figure 12 illustrates several rotational distributions at τ_{th}.

After threshold the $R-T$ transfer competes with the stimulated emission. The ratio R_{VJ} between the rates

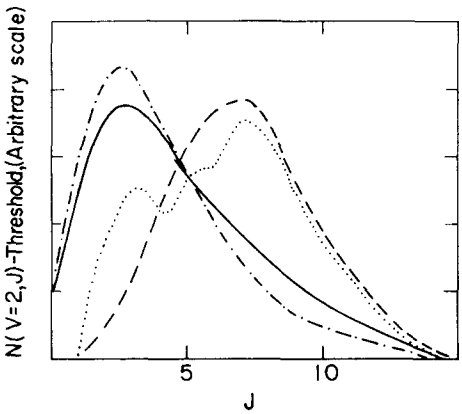

FIG. 12. Rotational distribution at $t=\tau_{th}$. ---, IRC; discharge, 1:10, $R-T$ (low pressure); $\tau_{th}=0.6$ μsec; ——, the same but with high $R-T$, $\tau_{th}=0.6$ μsec; -·-, IRC, flash, 1:10 high $R-T$, $\tau_{th}=3.5$ μsec; owing to the longer threshold time this distribution is closer to the thermal shape than in the case of discharge initiation. ···, IRC, flash, $R-T$ (low pressure) at $t=4$ μsec $\gtrsim \tau_{th}$. The irregular shape is due to the fact that lasing has just started in $P_{2\to1}$ (7) and $P_{3\to2}$ (2, 3).

by which stimulated emission and rotational relaxation deplete the vib–rotational level V,J is

$$R_{VJ} = \frac{c\sigma_{VJ}\Delta N_{VJ} q_{VJ}}{k(J\to)N_{VJ}M} \quad . \tag{25}$$

To estimate R_{VJ} we replace N_{VJ} and q_{VJ} by their quasi-steady-state values[92] ΔN_{th} and $P_{VJ}\tau$, respectively (P_{VJ} is the pumping rate at $t \gtrsim \tau_{th}$). Equation (25) then yields $R_{VJ} \sim 10$ and 1/30 for $V=2, J=5$ in the low and high pressure limits, respectively. Figure 13 illustrates three output patterns corresponding to F : $H_2 = 5:6$ with $M = 1.7$, 5.3, and 300×10^{-8} mole/cm^3, respectively. The corresponding values of $R_{V,J}$ (for $V=2, J=5$ at $t=2$ μsec) are about 3, 1, and 1/100, respectively

The different effects of moderate and enhanced rotational relaxation on τ_{th} and τ_q are indicated in Table V. In the first case the threshold behavior can be predicted from the data for no relaxation; the spread in τ_{th} is small, and all positive gain transitions lase simultaneously. The growth in the population inversion of specific transitions, before threshold, is governed by the pumping reaction $N_{VJ} \propto P(VJ)$. Therefore, the first lines to reach threshold can be determined from

$$(t<\tau_{th})\Delta N_{VJ} \propto \Delta P(V,J) = P(V,J-1) - [(2J+1)/(2J-1)]P(V-1,J) \ , \tag{26}$$

where $P(V,J)$ is the product state distribution in the pumping reaction (12). For the IRC distribution, (26) implies that the highest gain transitions are $P_{3\to2}(2,3)$ and $P_{2\to1}(5-9)$, as confirmed in Table V. Although $V=3$ is less populated than $V=2$, $P(V=3, J\leq3)$

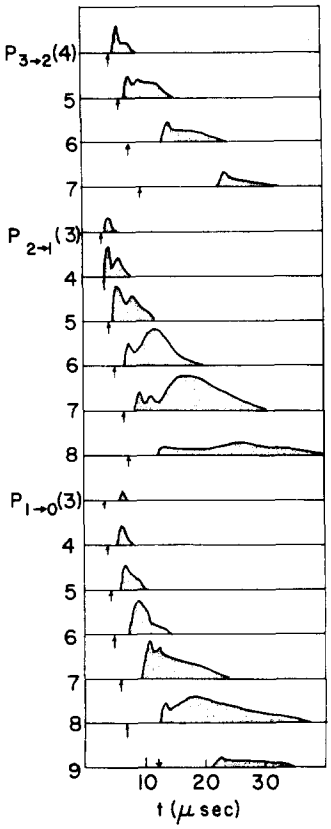

FIG. 14. Temporal evolution and relative intensities of P-branch transitions. Flash initiation, IRC product distribution, $F:H_2=1:10$, high $R-T$. The arrows indicate the threshold times of Ref. 31.

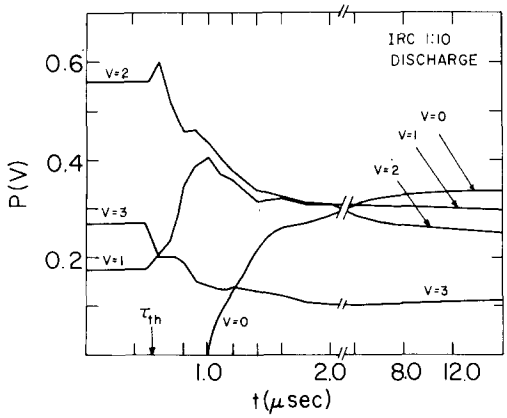

FIG. 16. Development in time of vibrational populations. Lasing begins in $V=3\rightarrow 2$ and $V=2\rightarrow 1$.

$\gg P(V=2, J\leq 4)$. In the high $R-T$ case, τ_{th} increases with J and the (time) overlap between the pulses is considerably smaller than in the normal $R-T$ case. The J shifting is particularly pronounced in the $V=3\rightarrow 2$ band. In the $V=2\rightarrow 1$ and $V=1\rightarrow 0$ bands, radiational cascades from higher vibrational levels interfere with the J shifting.

The differences between the two extremes of $R-T$ relaxation are particularly pronounced for the flash initiation–slow pumping mechanism. As a result of the slow pumping (in comparison to discharge), τ_{th} are longer, the spacings between τ_{th} of neighboring transitions are larger, and the overlap between individual pulses is smaller, mainly in the $P_{3\rightarrow 2}$ band. The temporal evolution of the laser pulses in the case of flash initiation (high $R-T$) is shown in Fig. 14. Note that here (as in all other cases characterized by high $R-T$) lasing begins in the $V=2\rightarrow 1$ band. Lasing from $V=3$ begins only after $V=2$ has been sufficiently depopulated by $V=2\rightarrow 1$ transitions as shown in Fig. 15. The development in time of $P(V)$ under normal $R-T$ conditions is depicted in Fig. 16.

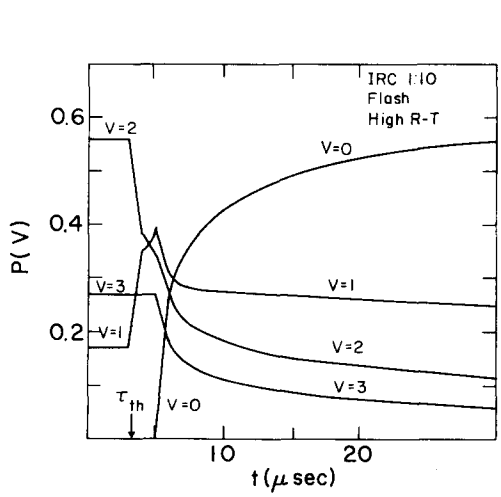

FIG. 15. Development in time of vibrational populations $P(V)=N_V/\Sigma N_V$. Lasing starts in the completely inverted band $V=2\rightarrow 1$. Most of the laser energy is extracted under partial inversion conditions, compare with Fig. 14.

Comparison of Figs. 14 and 15 indicates that in the high $R-T$ case, a major portion of the laser energy is extracted from partially inverted populations, i.e., when $P(V)<P(V-1)$. (The situation is similar for discharge initiation.)

Lasing terminates with $P(V)<P(V-1)$ also at low pressures, Fig. 16. However, the ratio $P(V)/P(V-1)$ is considerably smaller than in the former case. This fact is consistent with the result indicated in Table IV, that enhanced rotational relaxation improves the efficiency of the laser. A qualitative explanation to this behavior can be given as follows: The laser pulse terminates when the pumping rate falls to such a low value that the nonradiative losses prevent any of the ΔN_{VJ}'s to reach threshold, or simply when all $N_{VJ}\leq \Delta N_{th}$. $[\Delta N_{th}=(c\sigma_{VJ}\tau)^{-1}$ is inversely proportional to V but almost independent of J.] If the pressure is low, the $R-T$ transfer cannot couple the different rotational levels and lasing terminates independently in every transition, i.e., $\Delta N_{VJ}\simeq \Delta N_{th}$ for every V, J. In the other extreme, high pressures, lasing may continue until $\Delta N_{VJ*}\simeq \Delta N_{th}$, where J^* is the highest gain transition in the J-shifting sequence whereas $\Delta N_{VJ}<\Delta N_{th}$ for all $J<J^*$.

The improvement of the laser efficiency by enhanced rotational relaxation was also found for cw lasers[17] and other (not HF) chemical lasers.[18]

3. *Effect of V-R,T transfer*

As can be judged from Figs. 5–8 and Table IV, the $V-R, T$ deactivation processes reduce the total pulse energy but do not have a drastic effect on the spectral distribution of the laser output. In testing their influ-

ence no distinction was made between pure $V-T$ transfer (HF–H collisions) and (almost) pure $V-R$ transfer (HF–HF and HF–F collisions). Considering that $N_{HF}(t) = N_H(t)$ and that our k_{HF-H} is significantly larger than k_{HF-HF} (for most J's, Fig. 4), it is clear that the $V-R$ effect is partly suppressed by the $V-T$ transfer. In the early stages of the laser pulse HF–F collisions are the main cause for $V-R, T$ transfer. However, these have relatively low rate constants and cannot significantly compete with the intense stimulated emission. In addition, the $V-R$ rate constants for populating the high J levels in $V=2$ (originating in the low J's of $V=3$) are somewhat smaller than the rate constants for depopulating them [terminating at high J's in $V-1$, see Eq. (18), Fig. 4, and Table II]. This is reflected by the diminished laser intensity from several high J levels in $V=2$ and the somewhat enhanced intensity from similar levels in $V=1$ (in comparison to no relaxation, Fig. 7). These effects almost disappear when the $V-V$ and $R-T$ processes are also taken into account.

Based on approximate expressions for the $V-R, T$ rate constants formulated in Sec. II. C, we conclude that $V-R$ transfer cannot serve as an efficient pumping mechanism of high rotational levels. Only if $k(V \to V-1) \gg Vk(1 \to 0)$ would $V-R$ effects be expected in the laser output. [$k(V \to V-1 = V^2 k(1 \to 0)$ was suggested by Chen *et al.*[16] to account for their experimental data.]

4. Effect of V-V exchange

The results of the calculations indicate that the effects of $V-V$ exchange are pronounced only for F : H_2 = 5 : 6. This implies, as expected, that unless $[H_2] \gg [HF]$, HF–HF collisions are considerably more effective than HF–H_2 collisions.

The main findings about the $V-V$ processes are that they reduce the overall laser intensity $Q = \sum Q_V$ but increase the ratios $Q_{V \to V-1}/Q_{V-1 \to V-2}$ ($V = 3, 2$). These results are in accordance with the suggestion of Osgood *et al.*[83] regarding the important effect of HF anharmonicity. Specifically, both the asymmetry of the $V-V$ rate constants, Fig. 4, and the vibrational population ratios ($N_V N_V > N_{V-1} N_V$ for almost every t, Fig. 16) favor the $2,2 \to 3,1$; $1,1 \to 2,0$, and $2,1 \to 3,0$ transitions over the corresponding reverse transitions. This leads on the average to an increase in N_3 and N_0, hence enhancing lasing in the $V=3 \to 2$ band and reducing the lasing in the $V=1 \to 0$ and $V=2 \to 1$ bands. Since the general trend is of equalizing the N_V's, the overall laser intensity is smaller than in the case of no relaxation. This tendency is also reflected by the reduction in τ_q, Table IV.

To estimate the sensitivity of the results to the absolute values of the $V-V$ rates, several calculations, denoted as "low $V-V$" in Table IV, have been performed. The rate constants of (R. 6) were taken an order of magnitude smaller than in the general case. It is seen that the effect of $V-V$ transfer, although reduced, remains appreciable. Indirectly this implies that removal of the approximations involved in neglecting $V-V$ transfer to $V \gtrsim 4$ and in disregarding the temperature variations would not yield qualitatively different results. In fact, the errors resulting from these approximations have been tested in detail (for Cl + HBr → HCl + Br laser) and found to be small.[18]

B. Laser performance

1. Initial conditions and threshold behavior

The increase in pumping rate and total HF concentration in passing from F : H_2 = 1 : 10 to F : H_2 = 5 : 6 leads to shorter threshold times, longer pulse durations (as long as $V-V$ and $V-R, T$ processes are not taken into account), and larger output energies, Table IV. On the other hand, the larger H, F, HF concentrations in the F : H_2 = 5 : 6 case lead to a significant reduction in the total energy (in comparison to no relaxation). The spectral distributions of laser outputs corresponding to the same initial rotational distribution (IRC or statistical) are not very sensitive to the initial concentration ratio (also in the high $R-T$ case).[93]

In addition, the spectral distribution of the laser output does not markedly change when the laser is initiated by flash photolysis instead of discharge, compare Figs. 5 and 17. The total output energies corresponding to the two initiation methods are also similar, Table IV. The differences are displayed, as expected, mainly in the threshold behavior, Tables IV and V and Figs. 14 and 18.

Besides threshold times the pumping rate also determines the pattern of the relaxation oscillations.[92]

First order approximation to the frequency of these oscillations ω and to the decay time of their amplitude

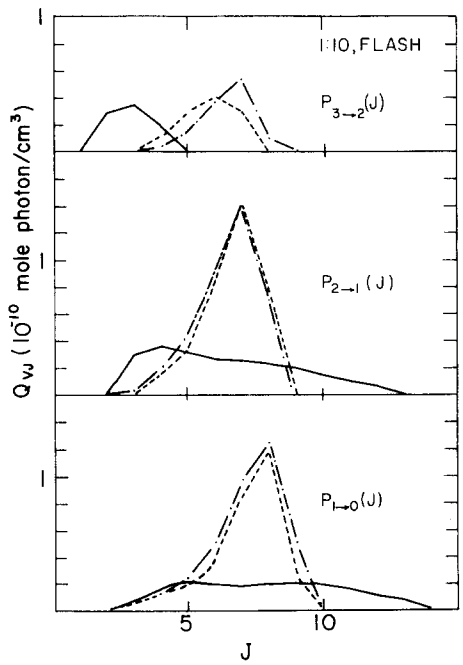

FIG. 17. Spectral distribution of laser output, flash initiation. -·-, IRC distribution high $R-T$. ——, IRC, $V-V+R-T+V-T$ (by H atoms). – – –, Thermal rotational distribution, high $R-T$. The difference in initial rotational distributions is cancelled by the fast rotational relaxation, compare Figs. 5 and 6 and Table II. The low pressure results are similar to those for discharge initiation, Fig. 5.

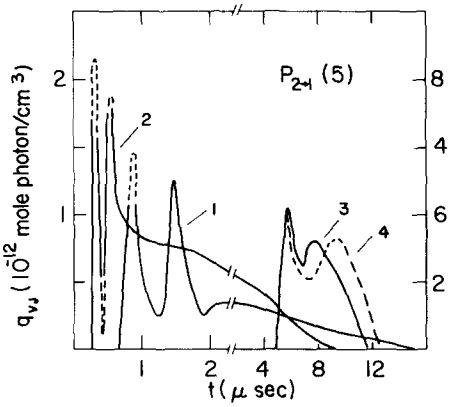

FIG. 18. Typical laser pulses; $P_{2\to1}$ (5) at different initial conditions. 1. IRC, discharge, 1:10 2. IRC, discharge, 5:6 (right-hand scale). 3. IRC, flash, 1:10.4. Thermal, flash, 1:10.

τ_d can be obtained from the linearized form of the rate equation for q_{vJ} [see, e.g., Refs. 4(h) and 92]. For a given P-branch transition, ω and τ_d are given by

$$\omega = [4cP\sigma - (c\tau P\sigma)^2]^{1/2}/2 \,, \tag{27}$$

$$\tau_d = 2/c\tau P\sigma \,, \tag{28}$$

where $\tau = 10^{-7}$ sec is the photon lifetime and $P = d\Delta N_{vJ}/dt$ is the pumping rate of the transition considered. Consider for example the $P_{2\to1}(5)$ line shown in Fig. 18 for which $\sigma = 1.6\times10^{-15}$ cm^2. To estimate ω and τ_d we take the pumping rate at $t \simeq \tau_{th}$. In the case of discharge initiation (Curves 1 and 2 in Fig. 18), τ_{th} is small and P is given, in a good approximation, by

$$P = \frac{d\Delta N_{2,5}}{dt} = k_1 \Delta P(2,5) N_{H_2}(0) N_F(0) \,, \tag{29}$$

where $\Delta N_{2,5} = N_{2,4} - (9/11)N_{1,5}$ and $\Delta P(2,5) = P(2,4) - (9/11)P(1,5)$. [$k_1$ is the pumping rate constant and $\Delta P(V,J)$ is the quantity on the rhs of (26)]. For the IRC distribution $P = 3.6\times10^{-6}$ and 3.0×10^{-5} mole/cm^3 · sec for F: H_2 = 1:10 and 5:6, respectively. Substitutions of these values into (27) and (28) yield $\omega \simeq 8\times10^6$ and 2.5×10^7 sec^{-1}, respectively. Equivalently, the separations between two adjacent maxima are $T = 2\pi/\omega \simeq 0.8$ μsec and 0.25 μsec. These values compare well with curves 1 and 2 in Fig. 18. The corresponding τ_d values are 0.2 μsec and 0.02 μsec. If (27) and (28) were exact, this would imply that the first peaks in Curves 1 and 2 of Fig. 18 had to be drawn much higher.

Equations (27) and (28) can also be used to estimate ω and τ_d for the case of flash initiation[94] (Curves 3, 4 in Fig. 18). Qualitatively, the relatively small ω and long τ_d are due to the slow pumping.

2. Efficiency

The quantities ϕ_q and ϕ_∞ given in Table IV represent the efficiency in terms of the average number of photons extracted from one HF molecule, or the photon yield

$$\phi_q = \frac{Q}{N_{HF}(\tau_q)} \,, \qquad \phi_\infty = \frac{Q}{N_{HF}(\infty)} = \frac{Q}{N_F(0)} \,. \tag{30}$$

The pumping reaction releases 35 kcal/mole. Taking $h\bar{\nu} \sim 3500$ cm^{-1} = 10 kcal/mole as an average photon energy [appropriate to $P_{2\to1}(7)$, $P_{1\to0}(9)$, or $P_{3\to2}(3)$] the chemical energy is ~ 3.5 photons/molecule. Hence, the chemical efficiency is $\eta = \phi/3.5$. The initial internal energy of the nascent HF molecules is $\langle E_V + E_R \rangle \simeq 26$ kcal/mole = 2.6 photons/molecule, which is the upper limit to ϕ. In the case of rotational equilibrium (most of) the initial rotational energy has been transferred to the heat bath[31,91] so that only $\langle E_V \rangle \simeq 23$ kcal/mole $\equiv$ 2.3 photons/molecules can be extracted as laser energy.

The maximal photon yield $\phi_q \sim \phi_\infty = 1.4$ obtains in the high $R-T$ cases, corresponding to about 60% of the available vibrational energy and 40% of the total chemical energy. Note, however, that these values represent upper limits to the actual efficiency since $V-V$ and $V-R, T$ processes were not taken into account here. Theoretically, the efficiency could be improved by taking lower ΔN_{th} (larger τ) values. This will allow $P(V)/P(V-1)$ to fall below the values given in Table IV, i.e., more efficient extraction of the vibrational energy from partially inverted populations. However, decrease in ΔN_{th} is accompanied by an increase in the pulse duration, i.e., in the effectivity of the relaxation processes.

The total pulse energy is given by $I = h\bar{\nu}VQ$, where V is the active laser volume. If $V = 2000$ cm^3 (as in Ref. 12) and $Q = 20\times10^{-10}$ mole · photon/cm^3 (as for IRC, discharge; 5:6, "All" in Table IV), we find $I \simeq 0.16$ J. The corresponding average power ($\Delta t \sim 10$ μsec) is $P = 16$ kW; the peak power is considerably higher, Fig. 18. For $Q = 4\times10^{-10}$ mole · photon/cm^3 (IRC, discharge, 1:10, all), $I \simeq 30$ mJ and $P \simeq 3$ kW.

3. Comparison with experiment

The limited accuracy of the presently available low pressure-discharge experimental data[12] does not allow a meaningful step-by-step comparison between experiment and theory (model calculations). The experimental values $\tau_{th} \sim 0.5$–1 μsec, $\tau_q \sim 15$ μsec, and $I \sim 50$ mJ compare reasonably well with the computed results for F: H_2 = 1:10. The agreement with respect to $Q_{V\to V-1}/Q_{V-1\to V-2}$ is poor; $Q_{3\to2}$; $Q_{2\to1}$; $Q_{1\to0} = 0.15:1.00:1.10$ experimentally and ~ 0.4:1.0:0.7 from the calculations. This discrepancy may indicate that the actual $V-R, T$ and $R-T$ processes are faster than assumed in the calculations. (A better agreement with experiment could be achieved by assuming, for example, $k_{V\to V-1} = V^2 k_{1,0}$, as suggested in Ref. 16). The absence of a few lines in the experimental spectrum [$P_{2\to1}(10)$ and $P_{1\to0}(10)$] points out that unknown factors in the experiment (e.g., absorption or electron impact phenomena) may also contribute to the discrepancy. The range and maxima of the experimental laser spectrum, shown schematically in Fig. 1, are typical for lasing under conditions of rotational disequilibrium.

If the intense lasing from high rotational levels is (as far as we rely on the rate constants used here) not due to $V-R$ transfer, it must be attributed either to direct chemical pumping or to secondary pumping processes such as electron impact. The first interpretation implies that the statistical distribution accounts for the

experimental output better than the IRC distributions (compare Figs. 1, 6, and 7). Yet, according to the rotational relaxation model described in Sec. II. C. 1, high rotational levels relax slowly and it seems very unlikely that the arrested relaxation IRC data do not correctly represent the original population of these levels. The possibility that the high rotational levels (such as in the statistical distribution) are pumped because the initial reactant energy in the laser experiments is considerably higher than that in the IRC experiments cannot be excluded. Another possibility for the population of high rotational levels may be pumping by electron impact. However, experiments[2] (carried out under different conditions than in Ref. 12) indicate that this is not a very probable explanation either. Finally, as mentioned above, it might be that we have used too small $V-R$ deactivation rates for $V \geq 2$. The inescapable conclusion from this analysis is that more refined laser experiments as well as detailed product state distribution measurements (corresponding to different reactant energies) still need to be performed in order to account for the fine details of the laser output.

We have not attempted to reproduce the detailed flash photolysis–high pressure data of Berry.[31] We adopted the flash profile from these experiments but did not try to vary parameters (e.g., the cross section for $CF_3I + h\nu \rightarrow CF_2I + F$ or the cavity parameters such as τ) so as to achieve good agreement with experiment. (The calculations were carried out mainly for the sake of comparison with the discharge results). Qualitatively the calculations agree with the experiments with respect to the number of lasing transitions, the small degree of overlap between adjacent $P_{V-V-1}(J)$ transition (mainly in $V = 3 \rightarrow 2$), the rise in τ_{th} with J (J shift), and the efficient extraction of laser energy from partially inverted populations. Figure 14 indicates that the calculations are in quantitative accord with the experimental results for τ_{th} of the first few lasing transitions but not with respect to τ_{th} or τ_q of later transitions. There are three main reasons for that difference. First, in the calculation corresponding to Fig. 14, $V-V$ and $V-R, T$ processes were not taken into account; their inclusion would lead to shorter pulses and smaller $Q_{V-V-1}/Q_{V-1-V-2}$ values (experimentally[31] $Q_{3-2} : Q_{2-1} : Q_{1-0} = 0.3 : 1.0 : 1.25$). Second, our ΔN_{th} is larger than the experimental. Third, the high sensitivity of the output pattern to the flash profile.[4] The good agreement with respect to τ_{th} of the first few oscillating transitions is due to the steep rise in ΔN before threshold. Our results confirm the assumption[31] that $\phi < 2$ photons/molecule.

IV. CONCLUDING REMARKS

By solving the laser rate equations it has been shown that the common assumption of instantaneous rotational relaxation in chemical lasers is not always adequate. Model calculations based on this assumption may overlook important features of the laser output pattern. Single line operation (only in the highest vibrational band) and J shifting are achieved only at high buffer gas pressures. In general, enhanced rotational relaxation increases the laser efficiency; $V-V$ exchange, largely due to the anharmonicity of the HF molecules, enhances the lasing from upper vibrational levels but reduces the overall intensity; $V-R, T$ processes reduce the intensity; $V-R$ transfer is not an efficient pumping route for high rotational levels to the extent that rates used in this analysis represent true HF energy transfer rates.

The reliability of the results is restricted by the accuracy of the rate constants employed in the calculations. For a more faithful modeling, further detailed information in needed, for example, about the temperature dependence of the pumping rate constants and the initial product state distribution; the J dependence of the relaxation rate constants; deactivation rate constants of high vibrational levels. Yet we believe that in spite of the limitations model calculations of the kind presented here are valuable, at least qualitatively. Moreover, in view of the rapidly accumulating data on state-to-state rate constants there is no inherent reason why such, and more accurate, calculations should not become a (rather inexpensive) routine tool. Obviously, for systems more complicated than HF (e.g., CO or DF–CO_2 lasers where multitudes of internal states can be populated) there will be a need for very efficient computational techniques and systematic error analysis methods on the one hand[95] and physically significant approximations on the other.

We intend to extend the present work in several directions: for example, to perform more accurate low pressure experiments with well specified initial conditions (including different initiation techniques); to experiment on similar systems such as $F + HCl \rightarrow HF + Cl$, which have the same exothermicity as (R. 1), in order to resolve the discrepancy between the laser output measurements and the calculations based on IRC distributions; to investigate the role of optical and spectroscopic factors.

ACKNOWLEDGMENTS

We thank H. Pummer, E. Keren, R. B. Gerber, J. Wanner, and R. D. Levine for many helpful discussions. One of us (A. B-S) acknowledges the kind hospitality of the M. P. I. in Garching.

*Now at the Department of Physical Chemistry, The Hebrew University, Jerusalem, Israel.

[1]K. L. Kompa and G. C. Pimentel, J. Chem. Phys. 47, 857 (1967).

[2](a) T. F. Deutch, Appl. Phys. Lett. **10**, 234 (1967); (b) *ibid.* **11**, 18 (1967).

[3]See, for example; R. A. Gerber, E. L. Patterson, L. S. Blair, and N. R. Greiner, Appl. Phys. Lett. 25, 281 (1974).

[4]The following list is a sample of theoretical models: (a) N. Cohen, T. A. Jacobs, G. Emanuel, and R. L. Wilkins, Int. J. Chem. Kinet. 1, 551, 1969; (b) J. R. Airey, J. Chem. Phys. 52, 156 (1970); (c) P. H. Corneil and J. V. V. Kasper, IEEE J. Quantum Electron. **QE-6**, 170 (1970); (d) R. L. Kerber, G. Emanuel, and J. S. Whittier, Appl. Opt. **11**, 1112 (1972); (e) G. Emanuel and J. S. Whittier, App. Opt. **11**, 2047 (1972); (f) S. N. Suchard, R. L. Kerber, G. Emanuel, and J. S. Whittier, J. Chem. Phys. 57, 5065 (1972); (g) R. L. Kerber, N. Cohen, and G. Emanuel, IEEE J. Quantum Electron. **QE-9**, 94 (1973); (h) S. D. Rockwood, J. E. Brau, W. A. Proctor, and G. H. Canavan, IEEE J. Quantum Electron. **QE-9**, 94 (1973); (i) A. N.

Oraevskii, Sov. Phys.-JETP 28, 744 (1969); (j) A. N. Chester and L. D. Hess, IEEE J. Quantum Electron. **QE-8**, 1 (1972); (k) M. J. Molina and G. C. Pimentel, IEEE J. Quantum Electron. **QE-9**, 64 (1973).

[5]J. C. Polanyi, Appl. Opt. Suppl. 2, 109 (1965).

[6]M. S. Dzhidzhoev, V. T. Plantonenko, and R. V. Khokhlov, Sov. Phys. Usp. 13, 247 (1970).

[7]N. G. Basov, V. I. Igoshin, E. P. Markin, and A. N. Oraevskii, Sov. J. Quantum Electron. 1, 119 (1971).

[8]K. L. Kompa, Topics Curr. Chem. 37, 1 (1973).

[9]B. F. Gordietz, A. I. Osipov, E. V. Stupechenko, and L. A. Shelepin, Sov. Phys. Usp. 15, 759 (1973).

[10]M. J. Berry, in *Molecular Energy Transfer*, edited by J. Jortner and R. D. Levine (Wiley, New York, 1975).

[11]M. J. Berry, Ann. Rev. Phys. Chem. 26, xxx (1975).

[12]H. Pummer and K. L. Kompa, Appl. Phys. Lett. 9, 356 (1972).

[13]T. D. Padrick and M. A. Gusinow, Appl. Phys. Lett. 22, 183 (1973).

[14]A. Ben-Shaul, G. L. Hofacker, and K. L. Kompa, J. Chem. Phys. 59, 4664 (1973). See also A. Ben-Shaul and G. L. Hofacker in *Handbook of Chemical Lasers*, edited by J. F. Bott and R. W. F. Gross (Wiley, New York, 1976).

[15]T. D. Padrick and M. A. Gusinow, Chem. Phys. Lett. 24, 270 (1974).

[16]H. L. Chen, R. L. Taylor, J. Wilson, P. Lewis, and W. Fyfe, J. Chem. Phys. 61, 306 (1974).

[17]L. H. Sentman, J. Chem. Phys. 62, 3523 (1975).

[18]E. Keren, R. B. Gerber, and A. Ben-Shaul (to be published).

[19]Preliminary reports of the present work were given in (a) U. Schmailzl, A. Ben-Shaul, and K. L. Kompa, IEEE J. Quantum Electron. **QE-10**, 753 (1974); (b) U. Schmailzl, Diplomarbeit, Max-Planck Institute Report, IPP IV/75.

[20]In addition to Ref. 12, see for example Ref. 8 and (a) T. V. Jacobson and G. H. Kimbell, Chem. Phys. Lett. 8, 309 (1971); (b) O. R. Wood, E. G. Burkhardt, M. A. Pollack, and T. J. Bridges, Appl. Phys. Lett. 18, 112 (1971); 18, 261 (1971); (c) W. G. Green and M. C. Lin, J. Chem. Phys. 54, 3223 (1971); (d) O. R. Wood and T. Y. Chang, Appl. Phys. Lett. 20, 77 (1972); (e) C. J. Ultee, Rev. Sci. Instrum. 42, 1174 (1971). In some of these works pure rotational, R-branch, and superadiant transitions have been observed.

[21]J. C. Polanyi and K. B. Woodall, J. Chem. Phys. 57, 1574 (1972).

[22]A. Ben-Shaul, Chem. Phys. 1, 244 (1973).

[23]R. L. Jaffe and J. B. Anderson, J. Chem. Phys. 54, 2224 (1971); 56, 682 (1972).

[24]J. T. Muckerman, J. Chem. Phys. 56, 2997 (1972). See also J. Chem. Phys. 54, 1155 (1971); 57, 3388 (1972).

[25]R. L. Wilkins, J. Chem. Phys. 57, 912 (1972).

[26]J. C. Polanyi and K. B. Woodall, J. Chem. Phys. 56, 1563 (1972).

[27]A. M. G. Ding and J. C. Polanyi, Chem. Phys. 10, 39 (1975).

[28]V. S. Mashkevich, *Laser Kinetics*, (Elsevier, New York, 1967); M. Sargent III, M. O. Scully, and W. E. Lamb Jr., Laser Physics (Addison-Wesley, Reading, MA 1974).

[29]R. E. Meredith and F. G. Smith, J. Quant. Spectrosc. 13, 89 (1973). See also J. M. Herbelin and G. Emanuel, J. Chem. Phys. 60, 689 (1974).

[30]H. Pummer, W. Breitfeld, H. Wedler, G. Klement, and K. L. Kompa, Appl. Phys. Lett. 22, 319 (1973).

[31]M. J. Berry, J. Chem. Phys. 59, 6229 (1973).

[32]$k(VJ\rightarrow)$ is negligible unless $E_{VJ}\sim E$. However, these levels are barely populated. Thus only reverse reactions from $V=3$ were considered and treated as loss terms (for convenience). Mass conservation was imposed.

[33]See, for example, (a) K. H. Homann, W. C. Solomon, J. Warnatz, H. Gg. Wagner, and C. Zetzsch, Ber. Bunsenges. Phys. Chem. 74, 585 (1970); (b) K. L. Kompa and J. Wanner, Chem. Phys. Lett. 12, 560 (1972); (c) A. Perski, J. Chem. Phys. 59, 3612 (1973); (d) V. I. Igoshin, L. V. Kulakov, and A. I. Nikitin, Sov. J. Quantum Electron. 3, 306 (1974) and references cited therein; (e) Ref. 31.

[34]N. Jonathan, C. M. Melliar-Smith, and D. H. Slater, Mol. Phys. 20, 593 (1971).

[35]H. W. Chang and D. W. Setser, J. Chem. Phys. 58, 2298 (1973).

[36]J. G. Moehlmann and J. D. McDonald, J. Chem. Phys. 62, 3061 (1975).

[37]R. D. Coombe and G. C. Pimentel, J. Chem. Phys. 59, 251 (1973); 59, 1535 (1973).

[38]T. P. Schafer, P. E. Siska, J. M. Parson, F. P. Tully, Y. C. Wong, and Y. T. Lee, J. Chem. Phys. 53, 3385 (1970).

[39]N. C. Blais and D. G. Truhlar, J. Chem. Phys. 58, 1090 (1973).

[40]R. L. Jaffe, J. M. Henry, and J. B. Anderson, J. Chem. Phys. 59, 1128 (1973).

[41]A. M. G. Ding, L. J. Kirsch, D. S. Perry, J. C. Polanyi, and J. L. Schreiber, Discuss. Faraday Soc. 55, 252 (1973).

[42]See, e.g., S. F. Wu, B. R. Johnson, and R. D. Levine, Mol. Phys. 25, 839 (1973). G. C. Schatz, J. M. Bowman, and A. Kuppermann, J. Chem. Phys. 58, 4023 (1973). See also J. C. Tully, J. Chem. Phys. 60, 3042 (1974). Surface crossing in $F+H_2\rightarrow HF+H$. Approximate three dimensional calculations based on the Born approximation have recently been performed by A. Kafri, Y. Shimony, R. D. Levine, and S. Alexander (to be published).

[43]A. Ben-Shaul, R. D. Levine, and R. B. Bernstein, J. Chem. Phys. 57, 5427 (1972).

[44]R. D. Levine and R. B. Bernstein, Acc. Chem. Res. 7, 393 (1974).

[45]R. D. Levine and R. B. Bernstein, in *Dynamics of Molecular Collisions*, edited by W. H. Miller (Plenum, New York, 1975).

[46]R. B. Bernstein and R. D. Levine, Adv. At. Mol. Phys. 11, xxx (1975).

[47]J. L. Kinsey, J. Chem. Phys. 54, 1206 (1971).

[48]N. Cohen, Aerospace reports TR-0172 (2779)-2, 1971, and TR-0073 (3430)-9, 1972.

[49]For a recent extensive review see S. Ormunde, Rev. Mod. Phys. 47, 193 (1975).

[50]Essentially the same model, (18), was tested by W. H. Duewer and D. W. Setser, J. Chem. Phys. 58, 2310 (1973).

[51]I. Procaccia and R. D. Levine, J. Chem. Phys. 63, 3181, 4261 (1975). See also M. Rubinson and J. I. Steinfeld, Chem. Phys. 4, 467 (1974).

[52]See, for example, W. H. Deuwer, J. A. Coxon, and D. W. Setser, J. Chem. Phys. 56, 4355 (1972); D. Kley and K. H. Welge, J. Chem. 49, 2870 (1968).

[53]For a review, see T. Oka, Adv. A. Mol. Phys. 9, 127 (1973).

[54]J. O. Hirschfelder, C. F. Curtiss, and R. B. Bird, *Molecular Theory of Gases and Liquids* (Wiley, New York, 1954).

[55]$\overline{Z}\sim 0.5\,Z_{HF-H_2}\sim 3\,Z_{HF-HF}\sim 1.1\,Z_{HF-H}\sim 2.5\,Z_{HF-F}$. Hence the approximation $ZN=\overline{Z}\overline{N}=$ constant is, tacitly, equivalent to the assumption that $N(HF-HF)\sim 6N(HF-H_2)$, etc. This implies that $P(2\rightarrow)\,(HF-HF)\sim 6\,P(2\rightarrow)\,(HF-H_2)\sim 1/2$, etc., which is, roughly, in accord with rotational relaxation measurements, Ref. 56.

[56]According to C. E. Baker, J. Chem. Phys. 46, 2846 (1967) $Z_{rot}(HF-HF)\sim 9$ at 400 °K. F. J. Zelznik and R. A. Svehla, J. Chem. Phys. 53, 632 (1970) predict $Z_{rot}=8$ and 5 for $T=400$ and 500 °K, respectively, while Agrawal and M. P. Saksena, J. Chem. Phys. 61, 848 (1974), have calculated $Z_{rot}=2.5$ and 1.8 for the same temperatures, respectively. The laser fluorescence measurements of L. M. Peterson, G. H. Lindquist, and C. B. Arnold, J. Chem. Phys. 61, 3480 (1974) correspond to $Z_{rot}\lesssim 1$. These authors found also that the $R-T$ rate decreases from $J=5$ to $J=4$ by a factor of ~ 1.5 and that $k_{HF-HF}\sim 6\,k_{HF-H_2}$.

[57]In fact, by appropriate choice of parameters, various (similar) models can account for the rotational relaxation pattern.

[58]M. A. Kwok and R. L. Wilkins, J. Chem. Phys. 60, 2189

(1974).
[59]R. L. Wilkins, J. Chem. Phys. 58, 2038 (1973).
[60]D. L. Thompson, J. Chem. Phys. 57, 4170 (1972).
[61]The validity of this and other conclusions from Refs. 59 and 60 should be judged subject to the reservations made by C. F. Bender, B. J. Garrison, and H. F. Schaefer III, J. Chem. Phys. 62, 1188 (1975), regarding the accuracy of the LEPS potentials employed in these trajectory calculations.
[62]See J. F. Bott and G. J. Wolga, Abstracts to the Fourth Conference on Chemical and Molecular Lasers, October, 1974. We thank the referee for drawing our attention to this reference.
[63]In general, $V \rightarrow T$ transfer is the major relaxation mechanism when the attacking atom is light, e.g., in H + HCl or H + HF collisions. $V \rightarrow R$ is the major mechanism when the attacking atom is heavy, e.g., in Cl + HCl or F + HF collisions. In addition to Refs. 59, 60, see, for example (for H + HCl, Cl + HCl collisions) (a) D. L. Thompson, J. Chem. Phys. 56, 3570 (1972) and (b) R. L. Wilkins, J. Chem. Phys. 63, 534 (1975). For F + HF collisions, see Refs. 66–69 below. (c) The general trend indicated here is also in agreement with the mass criterion of J. D. Kelley, J. Chem. Phys. 53, 3864 (1970), which predicts that in the limit of (coplanar) impulsive collisions A + BC the efficiency of V–R transfer increases with $m = M_A M_C [M_B (M_A + M_B + M_C)]$. For previous treatments see (d) C. B. Moore, J. Chem. Phys. 43, 2979 (1965); (e) G. A. Kapralova, E. E. Nikitin, and A. M. Chaikin, Chem. Phys. Lett. 2, 581 (1968).
[64]L. S. Blair, W. D. Breashears, and G. L. Schott, J. Chem. Phys. 59, 1582 (1973).
[65]J. A. Blauer and W. C. Solomon, Int. J. Chem. Kinet. 5, 553 (1973). [The results reported in this work and in Ref. 64 and about 5 times smaller than those reported in two previous studies: J. F. Bott and M. Cohen, J. Chem. Phys. 55, 5124 (1971) and W. C. Solomon, J. A. Blauer, F. G. Jaye, and J. G. and W. C. Solomon, J. A. Blauer, F. C. Yaye, and J. G. Huat, Int. J. Chem. Kinet. 3, 215 (1971)].
[66]H. K. Shin, Chem. Phys. Lett. 14, 64 (1972).
[67]D. L. Thompson, J. Chem. Phys. 57, 4165 (1972).
[68]R. L. Wilkins, J. Chem. Phys. 59, 698 (1973).
[69]R. L. Thommarson and G. C. Berend, Int. J. Chem. Kinet. 6, 597 (1974).
[70]The explicit J dependence is not mentioned in Refs. 67 and 68. Support of the (somewhat arbitrary) choice of a linear J dependence comes from findings on Br + HBr collisions. J. M. White and D. L. Thompson, J. Chem. Phys. 61, 719 (1974).
[71]About 30 experimental and theoretical papers on V–R, T and V–V transfer in HF, DF, and HF + DF mixtures have, so far, been published (see Ref. 49). We shall refer to some of these below.
[72]J. F. Bott and N. Cohen, J. Chem. Phys. 55, 3698 (1971).
[73]G. C. Berend and R. L. Thommarson, J. Chem. Phys. 58, 3203 (1973).
[74]H. K. Shin, Chem. Phys. Lett. 26, 450 (1974).
[75]H. K. Shin, Chem. Phys. Lett. 10, 81 (1971); J. Phys. Chem. 75, 1079 (1971).
[76]L. H. Sentman, Chem. Phys. Lett. 18, 493 (1973).
[77]This assumption is, at least, not in contradiction to the experimental results of J. F. Bott, J. Chem. Phys. 57, 96 (1972). See discussion on this point in Ref. 48.
[78]W. H. Green and J. K. Hancock, IEEE J. Quantum Electron. **QE-9**, 50 (1973); J. H. Hancock and W. H. Green, J. Chem. Phys. 57, 4515 (1972).
[79]S. S. Fried, J. Wilson, and R. L. Taylor, IEEE J. Quantum. Electron. **QE-9**, 59 (1973).
[80]J. J. Hinchen, J. Chem. Phys. 59, 233, 2224 (1973).
[81]T. A. Dillon and J. C. Stephenson, J. Chem. Phys. 58, 2056, 3849 (1973); Phys. Rev. A 6, 1460 (1972).
[82]R. D. Sharma and C. A. Brau, J. Chem. Phys. 50, 924 (1969).
[83]R. M. Osgood Jr., P. B. Sackett, and A. Javan, J. Chem. Phys. 60, 1464 (1974).
[84]J. F. Bott, J. Chem. Phys. 57, 96 (1972).
[85]J. F. Bott, Chem. Phys. Lett. 23, 335 (1973).
[86]C. E. Treanor, J. W. Rich, and R. G. Rehm, J. Chem. Phys. 48, 1798 (1968); K. N. C. Bray, J. Phys. B 1, 705 (1968); 3, 1515 (1970).
[87]C. B. Moore, Adv. Chem. Phys. 23, 41 (1973) and references cited therein.
[88]For example, all terms where $V_1 = V + 1$ and $V' = 0$. In addition, we ignore terms correspondong to $V, V \pm 1 \rightarrow V \mp 1, V$, in spite of the fact that in our case J is specified and there are nonvanishing contributions of the kind $k(V, V+1 \rightarrow V+1, V)$ $[N_{VJ} N_{V+1} - N_{V+1,J} N_V]$. These terms are zero when $N_{V,J}/N_{V+1,J} = N_V/N_{V+1}$ as, for example, in a state of rotational equilibrium.
[89]J. F. Bott and N. Cohen, J. Chem. Phys. 58, 4539 (1973).
[90]As distinguished from Eqs. (1) and (2), where it was convenient to use q_{VJ} for the $V, J \rightarrow V-1, J+1$ transition, the results are presented in the common "mixed" notation, i.e., $P_{V \rightarrow V-1}(J)$ and q_{VJ} correspond to the $V, J-1 \rightarrow V-1, J$ transition.
[91]A. Ben-Shaul, O. Kafri, and R. D. Levine, Chem. Phys. 10, 367 (1975).
[92]H. G. Unger, *Introduction to Quantum Electronics* (Pergamon, Oxford, 1970).
[93]This conclusion does not change very much even if instead of the "upper limit" rate constants for HF–H collisions of Ref. 58 considerably lower values are used in the modeling–Ref. 19b.
[94]R. N. Chester, J. Chem. Phys. 53, 3595 (1970).
[95]A fast integrating scheme is presented in Ref. 18. A method for estimating the sensitivity of the solutions of the master equations to uncertainties in the rate constants has been suggested by R. I. Cukier, C. M. Fortwin, K. E. Shuler, A. G. Petschek, and J. H. Schaiby, J. Chem. Phys. 59, 3873 (1973) and J. H. Schaiby and K. E. Shuler, J. Chem. Phys. 59, 3879 (1973).